DMD Fast Forward. Published on January 6, 2022 as DOI: 10.1124/dmd.121.000796
This article has not been copyedited and formatted. The final version may differ from this version.

Title

Usefulness of human jejunal spheroid-derived differentiated intestinal epithelial cells for the prediction of intestinal drug absorption in humans

Authors

Kazuyoshi Michiba, Kazuya Maeda, Osamu Shimomura, Yoshihiro Miyazaki, Shinji Hashimoto, Tatsuya Oda and Hiroyuki Kusuhara

Affiliations

Laboratory of Molecular Pharmacokinetics, Graduate School of Pharmaceutical Sciences, The University of Tokyo, Tokyo, Japan (K.Mi., K.Ma. and H.K.)

Laboratory of Pharmaceutics, School of Pharmacy, Kitasato University, Tokyo, Japan (K.Ma.)

Department of Gastrointestinal and Hepato-Biliary-Pancreatic Surgery, Faculty of Medicine, University of Tsukuba, Ibaraki, Japan (O.S., Y.M., S.H. and T.O.)

Downloaded from dmd.aspetjournals.org at ASPET Journals on April 19, 2024

DMD Fast Forward. Published on January 6, 2022 as DOI: 10.1124/dmd.121.000796
This article has not been copyedited and formatted. The final version may differ from this version.

Running title

Prediction of intestinal absorption using jejunal spheroids

Corresponding author

Kazuya Maeda, Ph.D.

Affiliation: Laboratory of Pharmaceutics, Kitasato University School of Pharmacy

Address: 5-9-1, Shirokane, Minato-ku, Tokyo 108-8641, Japan

Tel/Fax: +81-3-5791-6249; Email: maedak@pharm.kitasato-u.ac.jp

Hiroyuki Kusuhara, Ph.D.

Affiliation: Laboratory of Molecular Pharmacokinetics, Graduate School of Pharmaceutical Sciences, The University of Tokyo

Address: 7-3-1, Hongo, Bunkyo-ku, Tokyo 113-0033, Japan

Tel: +81-3-5841-4770; Fax: +81-3-5841-4766; Email: kusuhara@mol.f.u-tokyo.ac.jp

Numbers for manuscript elements

Text pages: 39

Number of Tables: 1

Number of Figures: 7

Number of References: 43

Number of Supplementary Tables: 5

Number of Supplementary Figures: 5

Number of words in the Abstract: 239/250

Number of words in the Introduction: 747/750

Number of words in the Discussion: 1,500/1,500

Downloaded from dmd.aspetjournals.org at ASPET Journals on April 19, 2024

DMD Fast Forward. Published on January 6, 2022 as DOI: 10.1124/dmd.121.000796
This article has not been copyedited and formatted. The final version may differ from this version.

Abbreviations

1,25-$[OH]_2D_3$, 1α, 25-dihydroxyvitamin D_3; 2D, two-dimensional; 3D, three-dimensional; ABC, ATP-binding cassette; BCRP, breast cancer resistance protein; CES, carboxylesterase; CYP, cytochrome P450; DMEM, Dulbecco's modified Eagle medium; ER, efflux ratio; Fa, fraction of oral drugs that enter the gut wall; FBS, fetal bovine serum; Fg, intestinal availability; Gly-Sar, glycylsarcosine; iPSC, induced pluripotent stem cell; LC-MS/MS, liquid chromatography–tandem mass spectrometry; OATP, organic anion transporting polypeptide; P_{app}, apparent permeability coefficient; PEPT1, peptide transporter 1; P-gp, P-glycoprotein; RT-qPCR, reverse transcription–quantitative polymerase chain reaction; SLC, solute carrier; SI, sucrase-isomaltase; TEER, transepithelial electrical resistance; UGT, uridine 5′-diphospho-glucuronosyltransferase

Downloaded from dmd.aspetjournals.org at ASPET Journals on April 19, 2024

DMD Fast Forward. Published on January 6, 2022 as DOI: 10.1124/dmd.121.000796
This article has not been copyedited and formatted. The final version may differ from this version.

Abstract

This study aimed to demonstrate the usefulness of human jejunal spheroid-derived differentiated intestinal epithelial cells as a novel *in vitro* model for clarifying the impact of intestinal drug-metabolizing enzymes and transporters on the intestinal absorption of substrate drugs in humans. Three-dimensional human intestinal spheroids were successfully established from surgical human jejunal specimens and expanded for a long period using L-WRN-conditioned medium, which contains Wnt3a, R-spondin 3, and noggin. The mRNA expression levels of intestinal pharmacokinetics-related genes in the human jejunal spheroid-derived differentiated intestinal epithelial cells were drastically increased over a 5-day period after seeding compared with those in human jejunal spheroids and were approximately the same as those in human jejunal tissue over a culture period of at least 13 days. Activities of typical drug-metabolizing enzymes (cytochrome P450 [CYP] 3A, CYP2C9, uridine 5′-diphospho-glucuronosyltransferase 1A, and carboxylesterase 2) and uptake/efflux transporters (peptide transporter 1/*SLC15A1*, P-glycoprotein, and breast cancer resistance protein) in the differentiated cells were confirmed. Furthermore, intestinal availability (Fg) values estimated from the apical-to-basolateral permeation clearance across cell monolayer showed a good correlation with the *in vivo* Fg values in humans for five CYP3A substrate drugs (Fg range, 0.35–0.98). In conclusion, the functions of major intestinal drug-metabolizing enzymes and transporters could be maintained in human jejunal spheroid-derived differentiated intestinal epithelial cells. This model would be useful for the quantitative evaluation of the impact of intestinal drug-metabolizing enzymes and transporters on the intestinal absorption of substrate drugs in humans.

Significance Statement

Limited information is available regarding the quantitative prediction of the impact of drug-metabolizing enzymes and transporters on the human intestinal absorption of substrates using *in vitro* assays with differentiated cells derived from human intestinal spheroids/organoids. We confirmed the functions of typical drug-metabolizing enzymes and

Downloaded from dmd.aspetjournals.org at ASPET Journals on April 19, 2024

transporters in human jejunal spheroid-derived differentiated intestinal epithelial cells and demonstrated that Fg values estimated from apical-to-basolateral permeation clearance across cell monolayers showed a good correlation with *in vivo* human Fg values for CYP3A substrate drugs.

Downloaded from dmd.aspetjournals.org at ASPET Journals on April 19, 2024

DMD Fast Forward. Published on January 6, 2022 as DOI: 10.1124/dmd.121.000796
This article has not been copyedited and formatted. The final version may differ from this version.

Introduction

Various drug-metabolizing enzymes and drug transporters that play major roles in the oral absorption of drugs are expressed in the small intestine (Xie et al., 2016; Müller et al., 2017). For example, cytochrome P450 (CYP) 3A, which is the most important drug-metabolizing enzyme in the small intestine, and P-glycoprotein (P-gp), which is a multispecific efflux transporter on the apical membrane, are responsible for limiting the intestinal absorption of a wide variety of drugs. They provide the site of saturation, leading to the nonlinear pharmacokinetics of drugs (Takano et al., 2016). Furthermore, inhibition and induction of intestinal CYP3A and P-gp led to significant changes in the bioavailability of their substrate drugs in humans (Holtbecker et al., 1996; Greiner et al., 1999; Kato, 2008; Fenner et al., 2009). Therefore, quantitative evaluation of the impact of drug-metabolizing enzymes and transporters on intestinal drug absorption is important in the process of drug development.

Various *in vitro* models have been developed to quantitatively assess intestinal drug absorption in humans. Currently, Caco-2 cells, which are an immortalized cell line derived from human colorectal adenocarcinoma, are widely used in drug development as a gold standard for the *in vitro* models. The apparent permeability coefficients (P_{app}) of drugs that are absorbed mainly by passive diffusion across Caco-2 cell monolayers were closely correlated with the fraction of orally administered drugs that enter the gut wall (Fa) in humans (Artursson and Karlsson, 1991). However, previous studies showed that expression levels of certain drug-metabolizing enzyme and transporter subtypes, such as CYP3A and peptide transporter (PEPT) 1, in Caco-2 cells are significantly lower than those in the human small intestine (Seithel et al., 2006; Nakamura et al., 2002).

We recently reported freshly isolated human jejunal sections mounted onto the Ussing chamber as an *in vitro* model to investigate the impact of transporters on the intestinal absorption of substrate drugs in humans (Michiba et al., 2021). The functions of major drug-metabolizing enzymes and uptake/efflux transporters were maintained in this model

Downloaded from dmd.aspetjournals.org at ASPET Journals on April 19, 2024

(Rozehnal et al., 2012; Sjöberg et al., 2013; Michiba et al., 2021). However, some limitations exist with regard to utilizing this experimental system in the process of drug development. For instance, limited and irregular availability of fresh human intestinal tissue, narrow time window to maintain the barrier integrity in epithelial cells and transporter functions (Michiba et al., 2021), and a lack of cryopreservation method of intestinal tissue.

In recent years, rapid progress has been made in research on the generation of human induced pluripotent stem cell (iPSC)-derived intestinal epithelial cells. The activities of major intestinal drug-metabolizing enzymes and transporters were confirmed in human iPSC-derived intestinal epithelial cells (Kodama et al., 2016; Yoshida et al., 2021). However, it was suggested that human iPSC-derived intestinal epithelial cells partly showed an immature phenotype compared with adult human small intestinal cells (Finkbeiner et al., 2015). While some studies reported methods to control the differentiation status (Kodama et al., 2016; Kabeya et al., 2018), further research is needed to realize the quantitative prediction of intestinal drug absorption in humans, especially for CYP3A substrate drugs (Kabeya et al., 2020).

Spheroids and organoids, which are three-dimensional (3D) culture systems, have been used in a wide range of research fields as a model that reflects functional properties of organs and maintains cellular characteristics (Corrò et al., 2020). Intestinal spheroid cultures allow the long-term culture of intestinal stem cells with the capability to differentiate into multiple lineages (Sato et al., 2009; VanDussen et al., 2015). Furthermore, two-dimensional (2D) monolayers, which can allow easy evaluation of transcellular drug transport, can be set up from 3D intestinal spheroids (van der Hee et al., 2018). Recently, Yamashita et al. (2021) successfully demonstrated 2D monolayers from biopsy-derived human duodenal organoids showed the functions of CYP3A, carboxylesterase (CES) 2, and P-gp, and its global gene expression profile was closer to that of the human duodenum than of Caco-2 cells. Thus, human intestinal spheroid/organoid-derived intestinal epithelial cells are expected to maintain the function of detoxification occurring in the human

Downloaded from dmd.aspetjournals.org at ASPET Journals on April 19, 2024

intestine. However, limited information is available regarding the overall performance of such an *in vitro* assay system using differentiated cells derived from human 3D-cultured intestinal stem cells from the viewpoint of quantitative prediction of the impact of drug-metabolizing enzymes and transporters on the human intestinal absorption of substrate drugs.

In the present study, we aimed to demonstrate the usefulness of human jejunal spheroid-derived intestinal epithelial cells for investigating the quantitative impact of intestinal drug-metabolizing enzymes and transporters on the intestinal absorption of substrate drugs in humans.

Downloaded from dmd.aspetjournals.org at ASPET Journals on April 19, 2024

DMD Fast Forward. Published on January 6, 2022 as DOI: 10.1124/dmd.121.000796
This article has not been copyedited and formatted. The final version may differ from this version.

Materials & Methods

Chemicals

Commercially available compounds, including stable isotope-labeled compounds, were used in all experiments (Supplementary Table 1). All other chemicals and reagents used for analyses were also commercially available and analytical-grade products.

Human jejunal tissue

Human intestinal tissues (approximately 5 cm normal jejunal tissue specimens) were obtained from clinical patients with pancreatic head tumors who underwent pancreatoduodenectomy at the University of Tsukuba Hospital, as in our previous study (Michiba et al., 2021). All experimental protocols regarding these jejunal sections were approved by the ethics committees of both the Graduate School of Pharmaceutical Sciences, University of Tokyo and the Faculty of Medicine, University of Tsukuba. Written informed consent prior to surgery was obtained from all patients. The excised jejunum was immediately put in ice-cold Dulbecco's modified Eagle medium (DMEM) (Thermo Fisher Scientific, Waltham, MA, USA) at the operating theater and transferred to the laboratory at the University of Tsukuba within 30 min. For establishing human intestinal spheroid cultures, the excised jejunum was put in an ice-cold washing medium (DMEM/F12; Merck, Darmstadt, Germany) supplemented with 10% fetal bovine serum (FBS; Thermo Fisher Scientific), 2 mM L-glutamine (Merck), 100 units/mL penicillin and 100 μg/mL streptomycin (Thermo Fisher Scientific), and transferred on ice to the laboratory at the University of Tokyo. Procedures for establishing human intestinal spheroid cultures were immediately performed on the same day. To stabilize mRNA in the freshly isolated human jejunal tissues, a small part of the excised jejunum sample was immediately put into RNA*later* solution (Thermo Fisher Scientific). This sample was transferred on dry ice to the laboratory at the University of Tokyo and preserved at −80 °C until analyses by reverse transcription–quantitative polymerase chain reaction (RT-qPCR).

Downloaded from dmd.aspetjournals.org at ASPET Journals on April 19, 2024

DMD Fast Forward. Published on January 6, 2022 as DOI: 10.1124/dmd.121.000796
This article has not been copyedited and formatted. The final version may differ from this version.

Establishment of human jejunal spheroids

L-WRN cells (CRL-3276), which are L-cells expressing Wnt3a, R-spondin 3, and noggin, were obtained from the American Type Culture Collection (Rockville, VA, USA). We followed protocols for the establishment of human intestinal spheroid cultures and the preparation of L-WRN conditioned medium (L-WRN CM) previously described by Miyoshi and Stappenbeck (2013). Briefly, approximately 1 cm^2 of jejunal tissue specimens was minced and incubated with collagenase solution (washing medium supplemented with 2 mg/mL collagenase type I powder [FUJIFILM Wako Pure Chemical, Osaka, Japan] and 50 μg/mL gentamicin [Thermo Fisher Scientific]) at 37 °C for 1 h. Crypts were isolated from tissue fragments by pipetting, filtering through a 100 μm strainer, and centrifuging at 200 *g* for 5 min. The pellets were gently resuspended in Matrigel (Corning, Corning, NY, USA), and 60 μL of the cell suspension was placed at the center of each well in a 6-well plate and spread carefully using pipette tips. The plate was incubated at 37 °C for 15 min to allow Matrigel to be polymerized. A total of 2 mL of 50% L-WRN CM (1:1 dilution with advanced DMEM/F12 [Thermo Fisher Scientific] supplemented with 20% FBS, 2 mM L-glutamine, 100 units/mL penicillin, and 100 μg/mL streptomycin) containing 10 μM Y-27632 (a Rho-associated protein kinase inhibitor, FUJIFILM Wako Pure Chemical) and 1 μM SB431542 (a transforming growth factor-β inhibitor, FUJIFILM Wako Pure Chemical) was added to each well. Primary spheroids were generated within 3–5 days. The medium was replaced with fresh 50% L-WRN CM every 2 days.

Passage and cryopreservation of human jejunal spheroids

Human jejunal spheroids were passaged every 5–7 days at ratios of 1:3–1:5 for maintenance. We followed the protocol for the passage of human intestinal spheroids previously described by Miyoshi and Stappenbeck (2013). Briefly, human jejunal spheroids at 5–7 days after passage were collected and dissociated into small cell clusters by scratching the Matrigel using pipette tips, incubating the Matrigel-cell mixture in TrypLE™

Downloaded from dmd.aspetjournals.org at ASPET Journals on April 19, 2024

Express (Thermo Fisher Scientific) at 37 °C for 5 min, and pipetting gently. The small cell clusters were gently resuspended in fresh Matrigel and 60 μL of the suspension was placed at the center of each well in a 6-well plate and spread carefully using pipette tips. The plate was incubated at 37 °C for 15 min to allow the Matrigel to be polymerized and 2 mL of 50% L-WRN CM containing 10 μM Y-27632 and 1 μM SB431542 was added to each well. The medium was replaced with fresh 50% L-WRN CM every 2 days.

For cryopreservation, human jejunal spheroids at 5–7 days after passage were collected and dissociated into small cell clusters as described above and centrifuged at 200 *g* for 5 min. The pellets were gently resuspended in BAMBANKER™ (Lymphotec, Tokyo, Japan) and the suspension was frozen at −80 °C. The frozen cell suspension was stored in cryotubes in a liquid nitrogen tank.

Generation of 2D monolayers of differentiated intestinal cells from human jejunal spheroids

We followed the protocol for the generation of 2D monolayers of differentiated intestinal cells previously described by VanDussen et al. (2015). Human jejunal spheroids at 6 days after passage were collected and dissociated into single cells by scratching the Matrigel using pipette tips, incubating the Matrigel-cell mixture in TrypLE™ Express at 37 °C for 15 min, and pipetting vigorously. The single cells were filtered using a 40 μm strainer and centrifuged at 200 *g* for 5 min. The pellets were resuspended in 50% L-WRN CM containing 10 μM Y-27632 and cells were seeded into 24-well plates or 24-well culture inserts (polyester membrane, 0.4 μm pore size; Corning) at a density of 2.5×10^5–7.5×10^5 cells/cm^2. The plates or inserts were precoated using 0.5% (vol/vol) Matrigel in advanced DMEM/F12 at 37 °C for 1–2 h. The medium was removed and replaced with 0% L-WRN CM (advanced DMEM/F12 supplemented with 20% FBS, 2 mM L-glutamine, 100 units/mL penicillin, and 100 μg/mL streptomycin without Wnt3a, R-spondin 3, and noggin) at 24 h after seeding. The medium was replaced with fresh 0% L-WRN CM every 2 days.

Downloaded from dmd.aspetjournals.org at ASPET Journals on April 19, 2024

DMD Fast Forward. Published on January 6, 2022 as DOI: 10.1124/dmd.121.000796
This article has not been copyedited and formatted. The final version may differ from this version.

Transepithelial electrical resistance (TEER) values were measured using Millicell ERS-2 (Merck). Resistance of the monolayer seeded on culture inserts was obtained by subtracting the blank resistance value from the measured resistance value and then multiplying the values by the culture area of a culture insert (0.33 cm^2).

Gene expression analysis

Total RNA was isolated from the human jejunal tissue sections and human jejunal spheroid-derived intestinal epithelial cells seeded on 24-well plates using ISOGEN II (NIPPON GENE, Tokyo, Japan). cDNA was synthesized using ReverTra Ace™ qPCR RT Master Mix with gDNA Remover (TOYOBO, Tokyo, Japan) according to the manufacturer's instructions. The mRNA expression levels of *ABCB1* (P-gp), *SLC15A1* (PEPT1), *CYP3A4*, and *sucrase-isomaltase* (*SI*) were determined by qPCR analyses using THUNDERBIRD™ SYBR® qPCR Master Mix (TOYOBO, Tokyo, Japan) and a CFX Connect Real-Time PCR Detection System (Bio-Rad Laboratories, Hercules, CA, USA). The mRNA expression levels were normalized to that of the glyceraldehyde-3-phosphate dehydrogenase gene. The sequences of primers for the detection of the abovementioned mRNAs are presented in Supplementary Table 2.

Measurement of the bidirectional transport of digoxin, fexofenadine, sulfasalazine, and rosuvastatin across human jejunal spheroid-derived intestinal epithelial cell monolayer

Digoxin and fexofenadine (5 μM each) were selected as P-gp substrates and sulfasalazine and rosuvastatin (5 μM each) as BCRP substrates to investigate the efflux transport mediated by P-gp and BCRP. PSC833 (5 μM) and Ko143 (5 μM) were selected as specific inhibitors of P-gp and BCRP, respectively. To examine the effects of these inhibitors on passive transcellular transport, antipyrine (1 μM) was selected as a passive transcellular marker. Lucifer yellow (10 μM) was used as a paracellular marker to evaluate the integrity of the cell monolayer.

Downloaded from dmd.aspetjournals.org at ASPET Journals on April 19, 2024

Prior to the addition of test compounds, the cell monolayers at 7 days after seeding on 24-well culture inserts were preincubated for 30 min with transport buffer containing 118 mM NaCl, 1.53 mM $CaCl_2$, 4.83 mM KCl, 0.96 mM KH_2PO_4, 1.20 mM $MgSO_4$, 5.00 mM D-glucose, 23.8 mM $NaHCO_3$, and 12.5 mM MES (MES transport buffer, adjusted to pH 6.5, for apical side) or 12.5 mM HEPES (HEPES transport buffer, adjusted to pH 7.4, for basolateral side) in the presence or absence of P-gp/BCRP inhibitor cocktail (added to both sides). The buffer volumes used for the apical and basolateral compartments were 0.4 mL and 1 mL, respectively. The bidirectional transport assay was initiated by replacing the buffer in the apical and basolateral compartments with fresh MES or HEPES transport buffer with or without test compounds in the presence or absence of P-gp/BCRP inhibitor cocktail (added to both sides). The cell monolayers were incubated at 37 °C for 2 h. At 30, 60, and 120 min after the addition of test compounds, aliquots of the buffer in the receiver compartment were collected and an equal volume of fresh MES or HEPES transport buffer was added. The collected samples were preserved at −20 °C until liquid chromatography–tandem mass spectrometry (LC-MS/MS) analyses.

Measurement of the apical-to-basolateral transport of cefadroxil across human jejunal spheroid-derived intestinal epithelial cell monolayer

Cefadroxil (10 μM) was selected as a PEPT1 substrate to evaluate PEPT1-mediated cellular uptake. An excess concentration of glycylsarcosine (Gly-Sar; 10 mM), which is a typical substrate of PEPT1, was used to saturate PEPT1. As mentioned above, antipyrine (1 μM) and lucifer yellow (10 μM) were added to the buffer in the donor compartment to confirm no effect on passive and paracellular transport.

Prior to the addition of test compounds, the cell monolayers at 7 days after seeding on 24-well culture inserts were preincubated for 30 min in MES or HEPES transport buffer in the presence or absence of Gly-Sar (added only to the apical side). Afterward, the transport assay was initiated by replacing the buffer in the apical and basolateral compartments with fresh MES transport buffer with test compounds and HEPES transport buffer without test

Downloaded from dmd.aspetjournals.org at ASPET Journals on April 19, 2024

compounds, respectively, in the presence or absence of Gly-Sar (added only to the apical side). The sampling of the buffer was carried out as described above.

Measurement of the metabolic activities of CYP3A, CYP2C9, UGT1As, and CES2 in human jejunal spheroid-derived intestinal epithelial cells

Midazolam (5 μM), diclofenac (10 μM), raloxifene (5 μM), and irinotecan (50 μM) were selected to evaluate the metabolic activities of CYP3A4/5, CYP2C9, uridine 5′-diphospho-glucuronosyltransferase (UGT) 1A, and CES2, respectively. Ketoconazole (10 μM), sulfaphenazole (50 μM), zafirlukast (50 μM), and loperamide (20 μM) were used as specific inhibitors of CYP3A4/5, CYP2C9, UGTs, and CES2, respectively.

Prior to the addition of test compounds, the cells at 5 days after seeding on 24-well plates were preincubated for 30 min in HEPES transport buffer in the presence or absence of ketoconazole, sulfaphenazole, zafirlukast, and loperamide. Afterward, metabolism assay was initiated by replacing the buffer with fresh HEPES transport buffer containing the substrates in the presence or absence of the corresponding inhibitor. The cells were incubated at 37 °C for 2 h. After the 2 h-incubation, the buffer and cells were collected to determine the amount of the major metabolites produced by the corresponding enzyme (1′-hydroxy midazolam, 4′-hydroxy diclofenac, raloxifene-4′-glucuronide, and SN-38). Cellular protein amounts were measured using the bicinchoninic acid method. The metabolic activity was normalized by the cellular protein amount.

Measurement of the apical-to-basolateral transport of midazolam, triazolam, alprazolam, felodipine, and nifedipine across human jejunal spheroid-derived intestinal epithelial cell monolayer

Midazolam, triazolam, alprazolam, felodipine, and nifedipine (1 μM each) were selected as CYP3A substrates (non-P-gp substrates) to investigate the effects of ketoconazole, which is a potent CYP3A inhibitor, and 1α, 25-dihydroxyvitamin D_3 (1,25-$[OH]_2D_3$), which is a typical CYP3A inducer, on the apical-to-basolateral transport across the cell monolayers.

Downloaded from dmd.aspetjournals.org at ASPET Journals on April 19, 2024

To induce CYP3A expression by 1,25-$(OH)_2D_3$, cell monolayers were treated with 10 nM 1,25-$(OH)_2D_3$ for 96 h before starting the transport assay.

Prior to the addition of the substrates, the cell monolayers at 9 days after seeding on 24-well culture inserts were preincubated for 30 min in MES or HEPES transport buffer in the presence or absence of ketoconazole (10 μM; added to both sides). The transport assay was initiated by replacing the buffer in the apical and basolateral compartments with fresh MES transport buffer with the substrates and HEPES transport buffer without the substrates in the presence or absence of ketoconazole (added to both sides), respectively. The cell monolayers were incubated at 37 °C for 2 h. At 30, 60, and 120 min after the addition of the substrates, aliquots of the buffer in the receiver compartment were collected and an equal volume of fresh HEPES transport buffer was added. After 2 h-incubation, the buffer in the donor compartment and cells were collected to determine the amount of the major metabolites formed by CYP3A (1′-hydroxy midazolam, α-hydroxy triazolam, α-hydroxy alprazolam, dehydro-felodipine, and dehydro-nifedipine).

Analytical methods for determining the concentration of test compounds

Quantification of all test compounds except lucifer yellow was performed using QTRAP® 5500 LC-MS/MS System (AB SCIEX, Foster City, CA, USA) equipped with Nexera ultra-high performance liquid chromatography (UHPLC) (Shimadzu, Kyoto, Japan). Samples were mixed with three volumes of acetonitrile containing internal standards. The solution was vortexed and centrifuged at 20,000 *g* for 5 min and the supernatant was injected into the LC-MS/MS system. An Atlantis T3 C18 column (3 μm, 2.1 mm × 50 mm; Waters Corp., Milford, MA, USA) was used for the chromatographic separation of analytes and the column temperature was maintained at 40 °C. The mobile phase was distilled water containing 0.1% formic acid (A) and acetonitrile containing 0.1% formic acid (B). The flow rate was 0.4 mL/min, and the injection volume was 10 μL. The details of the HPLC conditions are summarized in Supplementary Table 3. The mass spectrometer with electrospray ionization was operated in both positive and negative multiple-reaction

Downloaded from dmd.aspetjournals.org at ASPET Journals on April 19, 2024

monitoring modes. The details of the multiple-reaction monitoring conditions are summarized in Supplementary Table 4.

The concentration of lucifer yellow was measured using a fluorescence microplate reader (Infinite® 200, excitation wavelength 428 nm, emission wavelength 536 nm; TECAN, Männedorf, Switzerland).

Data analysis

The apparent permeability coefficient (P_{app}; cm/s) was calculated according to Eq. (1):

$$P_{app} = \frac{dQ}{dt} \times \frac{1}{A \times C_0} \quad (1)$$

where dQ/dt, A, and C_0 represent the amount of the test compound transported to the receiver compartment per unit time when the linearity of its time-dependent transport was apparently maintained, the culture area of the culture insert membrane (0.33 cm^2), and the initial concentration of test compound in the donor compartment, respectively.

The efflux ratio (ER) was calculated according to Eq. (2):

$$Efflux\ ratio = \frac{P_{app,BtoA}}{P_{app,AtoB}} \quad (2)$$

where $P_{app,BtoA}$ and $P_{app,AtoB}$ represent the apparent permeability coefficient in the basolateral-to-apical direction and the apical-to-basolateral direction, respectively.

The intestinal availability (Fg) of CYP3A substrates was calculated using the following equations:

$$CL_{AtoB} = PS_1 \times \frac{PS_3}{PS_2 + PS_3 + CL_{met}} \quad (3)$$

$$CL_{AtoB}\ (-inh) = \frac{PS}{2 + \frac{CL_{met}}{PS}} \quad (4)$$

$$CL_{AtoB}\ (+inh) = \frac{PS}{2} \quad (5)$$

$$Fg = \frac{PS_3}{PS_3 + CL_{met}} = \frac{1}{1 + \frac{CL_{met}}{PS}} = \frac{1}{2\frac{CL_{A\ to\ B}\ (+inh)}{CL_{A\ to\ B}\ (-inh)} - 1} \quad (6)$$

where CL_{AtoB}, PS_1, PS_2, PS_3, and CL_{met} represent the transcellular transport clearance in the apical-to-basolateral direction, the intrinsic passive permeation clearance in the apical-to-cell direction, the intrinsic passive permeation clearance in the cell-to-apical direction,

Downloaded from dmd.aspetjournals.org at ASPET Journals on April 19, 2024

the intrinsic passive permeation clearance in the cell-to-basolateral direction, and the intrinsic metabolic clearance mediated by CYP3A, respectively. $CL_{AtoB}(-inh)$ and $CL_{AtoB}(+inh)$ represent the apical-to-basolateral transcellular transport clearance in the absence and presence of ketoconazole, respectively. To simplify the mathematical handling, assuming the intrinsic passive permeation clearance in each process was the same ($PS_1 = PS_2 = PS_3 = PS$) and the metabolic clearance mediated by CYP3A in the presence of ketoconazole was zero ($CL_{met} = 0$) in Eq. (3) because of its potent inhibitory effect, $CL_{AtoB}(-inh)$, $CL_{AtoB}(+inh)$, and Fg were simply described using Eqs (4)–(6), respectively.

Statistical analysis

Results are presented as the mean ± standard deviation. Statistical significance of the differences in the mean values between the data for two groups and among the data for three or more groups was assessed using unpaired Student's *t*-test and analysis of variance followed by Tukey's test, respectively. All statistical analyses were performed using GraphPad Prism (version 9.2; GraphPad Software, San Diego, CA, USA). Statistical significance was defined at $p < 0.05$.

Downloaded from dmd.aspetjournals.org at ASPET Journals on April 19, 2024

DMD Fast Forward. Published on January 6, 2022 as DOI: 10.1124/dmd.121.000796
This article has not been copyedited and formatted. The final version may differ from this version.

Results

Establishment of human intestinal spheroids and generation of 2D cell monolayers from 3D spheroids

We successfully established human intestinal spheroids from surgical jejunal specimens and generated 2D cell monolayers from 3D spheroids according to the protocols previously described by Miyoshi and Stappenbeck (2013) and VanDussen et al. (2015), respectively (Fig. 1). Intestinal spheroids were expanded in 50% L-WRN CM containing 10 μM Y-27632 and 1 μM SB431542 and passaged every 5–7 days at ratios of 1:3–1:5. Under our culture condition, intestinal spheroids could be normally cultured over at least 25 passages. To generate 2D monolayer cultures from 3D spheroids, 6-day cultured intestinal spheroids were collected from the Matrigel, enzymatically dissociated into single cells, and plated onto Matrigel-precoated cell culture plates or inserts. To avoid anoikis, the cells were incubated with 10 μM Y-27632 over the first 24 h after seeding. To differentiate the cells, Wnt3a, R-spondin 3, and noggin were removed at 24 h after seeding, and the medium was replaced with fresh 0% L-WRN CM every 2 days.

Culture period-dependent mRNA expression levels of enzymes and transporters and TEER values in human jejunal spheroid-derived differentiated intestinal epithelial cells

To investigate the appropriate timing for metabolism/transport assays with human jejunal spheroid-derived differentiated intestinal epithelial cells, mRNA expression levels of *ABCB1* (P-gp), which is an efflux transporter on the apical membrane; *SLC15A1* (PEPT1), which is an uptake transporter on the apical membrane; *CYP3A4*, which is the most abundant intestinal CYP enzyme; and *SI*, which is a typical matured enterocyte marker, were monitored over the culture period until 13 days.

Over a 5-day period after seeding, human jejunal spheroid-derived differentiated intestinal epithelial cells showed a drastic increase in the mRNA expression levels of *ABCB1* (3.8-fold), *SLC15A1* (21-fold), *CYP3A4* (63-fold), and *SI* (24-fold) compared with

Downloaded from dmd.aspetjournals.org at ASPET Journals on April 19, 2024

DMD Fast Forward. Published on January 6, 2022 as DOI: 10.1124/dmd.121.000796
This article has not been copyedited and formatted. The final version may differ from this version.

those in undifferentiated human jejunal spheroids at 6 days after passage (Fig. 2A–D). At 5 days after seeding, the ratio of mRNA expression level in differentiated intestinal epithelial cells to that in intact human jejunal tissue was 2.17 for *ABCB1*, 0.88 for *SLC15A1*, 1.92 for *CYP3A4,* and 0.74 for *SI*. Moreover, their expression levels were maintained at approximately the same levels as 5 days after seeding until 11 days after seeding and started to gradually decrease at 13 days after seeding. These findings suggested that this cell system is expected to maintain the functions of P-gp, PEPT1, and CYP3A4 until 11 days after cell seeding.

In addition, TEER values were measured to determine the integrity of the cell monolayer. For human jejunal spheroid-derived differentiated intestinal epithelial cells, TEER values reached approximately 300 Ω cm^2 by 5 days after seeding and remained steady at least until 13 days after seeding (Fig. 2E).

P-gp and BCRP-mediated transport in human jejunal spheroid-derived differentiated intestinal epithelial cells

To investigate whether the functions of P-gp and BCRP, which are typical intestinal efflux transporters, were maintained in human jejunal spheroid-derived differentiated intestinal epithelial cells, we evaluated the bidirectional transport of digoxin, fexofenadine, sulfasalazine, and rosuvastatin in the presence or absence of a mixture of PSC833 and Ko143. In parallel, the bidirectional transport of antipyrine and lucifer yellow were evaluated to confirm no effect of P-gp/BCRP inhibitor cocktail on the transport of non-P-gp/BCRP substrates across the cell monolayer.

For all the tested P-gp and BCRP substrate drugs, the basolateral-to-apical transport was significantly higher than that in the opposite direction and was clearly suppressed in the presence of P-gp/BCRP inhibitor cocktail (Fig. 3A–D and G–J). The ERs of digoxin (26), fexofenadine (5.2), sulfasalazine (22), and rosuvastatin (2.8) decreased to 0.65, 0.97, 1.5, and 0.65 after incubation with P-gp/BCRP inhibitor cocktail, respectively. In contrast, no significant difference in the bidirectional transport of antipyrine and lucifer yellow was

Downloaded from dmd.aspetjournals.org at ASPET Journals on April 19, 2024

DMD Fast Forward. Published on January 6, 2022 as DOI: 10.1124/dmd.121.000796
This article has not been copyedited and formatted. The final version may differ from this version.

observed regardless of the presence of P-gp/BCRP inhibitor cocktail (Fig. 3E, F, K, and L). These findings suggested that the transport activities of P-gp and BCRP were confirmed in human jejunal spheroid-derived differentiated intestinal epithelial cells.

PEPT1-mediated transport in human jejunal spheroid-derived differentiated intestinal epithelial cells

To investigate whether the function of PEPT1, which is an intestinal uptake transporter for peptides, was retained in human jejunal spheroid-derived differentiated intestinal epithelial cells, we evaluated the apical-to-basolateral transport of cefadroxil in the presence or absence of excess concentration of Gly-Sar.

The apical-to-basolateral transport of cefadroxil was significantly decreased in the presence of 10 mM of Gly-Sar (Fig. 4A and D). In contrast, no significant difference was noted in the apical-to-basolateral transport of antipyrine and lucifer yellow regardless of the presence of 10 mM Gly-Sar (Fig. 4B, C, E, and F). These findings suggested that the transport activity of PEPT1 was retained in human jejunal spheroid-derived differentiated intestinal epithelial cells.

CYP3A4/5, CYP2C9, UGT1As, and CES2-mediated metabolic activities in human jejunal spheroid-derived differentiated intestinal epithelial cells

To investigate whether the functions of CYP3A4/5, CYP2C9, UGT1As, and CES2, which are typical intestinal drug-metabolizing enzymes, were maintained in human jejunal spheroid-derived differentiated intestinal epithelial cells, marker reactions for these enzymes (midazolam 1′-hydroxylation for CYP3A4/5, diclofenac 4′-hydroxylation for CYP2C9, raloxifene 4′-glucuronidation for UGT1As, and irinotecan hydrolysis for CES2) were observed in the presence or absence of the corresponding enzyme inhibitors.

The production of metabolites (1′-hydroxy midazolam, 4′-hydroxy diclofenac, raloxifene-4′-glucuronide, and SN-38, respectively) was clearly observed and significantly decreased in the presence of the corresponding enzyme inhibitors (Fig. 5). These findings suggested

Downloaded from dmd.aspetjournals.org at ASPET Journals on April 19, 2024

that the metabolic activities of CYP3A4/5, CYP2C9, UGT1As, and CES2 were confirmed in human jejunal spheroid-derived differentiated intestinal epithelial cells.

Predictability of human Fg values of CYP3A substrate drugs estimated using human jejunal spheroid-derived differentiated intestinal epithelial cells

To investigate whether human jejunal spheroid-derived differentiated intestinal epithelial cells would be a useful tool for the quantitative evaluation of Fg values for substrate drugs of CYP3A, which is the most important drug-metabolizing enzyme in terms of intestinal drug metabolism, we evaluated the correlation between the estimated Fg values of CYP3A substrate drugs from *in vitro* assays using human jejunal spheroid-derived differentiated intestinal epithelial cells and *in vivo* ones obtained from the literature.

Initially, we investigated the effects of ketoconazole (a potent CYP3A inhibitor) and 1,25-$(OH)_2D_3$ (a typical CYP3A inducer) on the apical-to-basolateral transport of five CYP3A substrate (non-P-gp substrate) drugs (midazolam, triazolam, alprazolam, felodipine, and nifedipine). For CYP3A substrate drugs with relatively large first-pass metabolism, such as felodipine and midazolam, the apical-to-basolateral transport was increased in the presence of ketoconazole, while it was decreased in the presence of 1,25-$(OH)_2D_3$ (Fig. 6A–J). However, the metabolite production of these CYP3A substrate drugs was significantly decreased in the presence of ketoconazole and significantly increased in the presence of 1,25-$(OH)_2D_3$ (Fig. 6K–O).

Then, Fg values were estimated with Eqs (3)–(6) using the apical-to-basolateral permeation clearances in the presence or absence of ketoconazole. Table 1 shows a summary of the estimated and *in vivo* Fg values for the five CYP3A substrate drugs. The data points for these CYP3A substrate drugs mapped close to the identity line. Moreover, the data points were shifted to the left, away from the identity line in the presence of 1,25-$(OH)_2D_3$, i.e., the estimated Fg values decreased because of the increase in CYP3A-mediated metabolism (Fig. 7).

Downloaded from dmd.aspetjournals.org at ASPET Journals on April 19, 2024

DMD Fast Forward. Published on January 6, 2022 as DOI: 10.1124/dmd.121.000796
This article has not been copyedited and formatted. The final version may differ from this version.

Discussion

In this study, we aimed to demonstrate the usefulness of human jejunal spheroid-derived differentiated intestinal epithelial cells for investigating the quantitative impact of intestinal drug-metabolizing enzymes and transporters on the intestinal absorption of substrate drugs in humans.

We successfully developed human jejunal spheroid-derived differentiated intestinal epithelial cells, which retained the functions of multiple intestinal drug-metabolizing enzymes and transporters, without using any complicated differentiation procedures or specialized devices (Fig. 1). Human jejunal spheroids could be reproducibly established from human jejunal specimens obtained from several independent subjects and efficiently expanded over a long period (> 25 passages) in 50% L-WRN CM. In addition, differentiated intestinal epithelial cell monolayers could be prepared just by the withdrawal of Wnt3a, R-spondin 3, and noggin from the medium in a short period (within 1 week) (Fig. 2) compared with the time taken using Caco-2 cells (2–3 weeks) (Markowska et al., 2001) and human iPSC-derived intestinal epithelial cells (3–4 weeks) (Kabeya et al., 2020; Kawai et al., 2020). Most importantly, the functions of a wide variety of drug-metabolizing enzymes, such as CYP enzymes, phase II enzymes, and non-CYP phase I enzymes, as well as efflux/uptake transporters, were clearly confirmed in this system (Figs 4 and 5). Furthermore, the mRNA expression levels of multiple intestinal drug-metabolizing enzymes and transporters, except for *SLC10A2*, in this model were within a range of 4.1-fold compared with those in human jejunal tissues (Supplementary Fig. 1). Though primary human enterocytes have also been recently obtained from commercial sources, their utilization as an *in vitro* model for the characterization of drug intestinal absorption remains impractical because of the limited availability of cells and the difficult preparation of 2D monolayers on culture dishes or inserts. However, our simple protocol enables long-term propagation of intestinal stem cells with differentiation capability and routine use of human differentiated intestinal epithelial cells that are suitable for pharmacokinetic research.

Downloaded from dmd.aspetjournals.org at ASPET Journals on April 19, 2024

We successfully demonstrated that Fg values estimated in this system were well-correlated with the previously reported values in humans for CYP3A substrate drugs (Fig. 7). Kabeya et al. (2020) reported the correlation between the P_{app} values of various drugs across human iPSC-derived intestinal epithelial cells and the reported product of fraction absorbed and intestinal availability (FaFg) in humans. However, P_{app} values of CYP3A substrate drugs markedly deviated from the correlation curve for other drugs, leading to speculation that CYP3A activity in the cells was not high enough to account for the clinically relevant FaFg. Theoretically, when drugs undergo significant intracellular metabolism, luminal flow rate (Q) and absorption clearance (CL_{ab}) also need to be considered to associate CL_{AtoB} with FaFg (Supplementary Figs 2 and 3). For simplicity, we calculated Fg according to Eq. (6) under the assumption that passive membrane permeation clearance was identical ($PS_1 = PS_2 = PS_3$) and metabolic clearance mediated by CYP3A in the presence of ketoconazole was zero ($CL_{met} = 0$). Felodipine and midazolam were the only drugs whose apical-to-basal P_{app} were significantly higher in the presence of ketoconazole under normal conditions (Fig. 6F and I). Hence, we conducted Fg estimation based on the difference in CL_{AtoB} of all tested drugs in the presence or absence of ketoconazole regardless of its statistical significance (Fig. 6F–J). Comparison of the total amount of parent drugs transferred to the basolateral compartment and the total amount of metabolites produced during the study is another approach to estimate Fg. Our findings enabled reasonable estimation of Fg values (Supplementary Fig. 4 and Supplementary Table 5). This method assumes that all the major drug metabolites are quantified and secondary metabolism of metabolites is negligible during the study. However, this approach is sometimes difficult to apply for new drug candidates because of limited information on their whole metabolic pathways.

This system maintained the transport activities of PEPT1, P-gp, and BCRP (Figs 3 and 4). The ERs of digoxin, fexofenadine, sulfasalazine, and rosuvastatin were 26, 5.2, 22, and 2.8, respectively (Fig. 3). The corresponding values in freshly isolated human jejunum were

Downloaded from dmd.aspetjournals.org at ASPET Journals on April 19, 2024

4.0, 6.4, 19, and 3.1, respectively (Michiba et al., 2021). Thus, these values, except for that of digoxin, were consistent in both cases. Further accumulation of experimental data is necessary to conclude that this system can be a novel *in vivo*-relevant cellular model for drug absorption of P-gp and BCRP substrates in humans. P-gp and BCRP substrate drugs showed a drastic decrease in the basolateral-to-apical transport in the presence of the P-gp/BCRP inhibitor cocktail, although almost no changes were observed in the apical-to-basolateral transport of the drugs. Because a previous report suggested that a balance between membrane permeation clearances of drugs across the apical and basolateral membranes can modify the pattern of alteration in the bidirectional transport clearances when the apical efflux transport is inhibited (Mizuno et al., 2003), further attention must be paid to the change in each membrane transport process at both sides of the cells.

Though the present study highlighted the successful application of human intestinal spheroid-derived differentiated intestinal epithelial cells for the characterization of oral absorption of drugs in the process of drug development, this study still has some limitations.

First, human intestinal spheroids used in this study were established only from the jejunum. It is well-known that some intestinal drug-metabolizing enzymes and transporters show region-specific gene expression profiles (Drozdzik et al., 2014; Fritz et al., 2018). Several studies suggested that intestinal spheroids/organoids established from different regions of the intestine (i.e., the duodenum, jejunum, and ileum) retained the region-specific gene expression profiles of their origin (Middendorp et al., 2014; Meran et al., 2020). Thus, this system is expected to be a novel cellular model possessing a region-specific gene expression profile. However, more in-depth research regarding this aspect is required. Second, human intestinal spheroids used in this study were established from a limited number of donors. Therefore, further studies are needed to judge the applicability of this system to the evaluation of interindividual variation of intestinal drug absorption in humans by collecting various batches of human intestinal spheroids originating from

Downloaded from dmd.aspetjournals.org at ASPET Journals on April 19, 2024

independent donors. As in the case of human liver microsomes and hepatocytes, this system may serve as an *in vitro* model for studying the interindividual difference in drug absorption, for instance, the difference due to genetic polymorphisms of *BCRP*. The area under the plasma concentration versus time curve values after oral administration (AUC_{po}) of BCRP substrate drugs, such as sulfasalazine, rosuvastatin, and topotecan, were approximately 1.3–2.4 times higher in homozygotes of *ABCG2* c.421C>A, which is associated with lower protein expression and transport function, than in those without this mutation (Sparreboom et al., 2005; Zhang et al., 2006; Urquhart et al., 2008). When crypts can be collected from the subjects that show interindividual differences in drug absorption, this system can be used as an *in vitro* model to uncover the underlying mechanisms. However, even with the use of cells from the same origin, interexperimental variation in the CYP3A-mediated metabolic activity was observed (approximately 3-fold; Supplementary Fig. 5). In future, for precise evaluation of the intrinsic interbatch difference in metabolic/transport activity, the assay protocol needs to be improved to achieve high quantitative reproducibility.

We successfully demonstrated that this system maintains the activities of drug transporters such as P-gp and BCRP, and drug metabolizing enzymes such as CYP3A and UGT1As. There are drugs whose FaFg are determined by multiple transporters and metabolic enzymes. For instance, many dual substrates of CYP3A and P-gp have been identified because of their overlapping substrate specificities (Takano et al., 2016), and thus further studies should be needed whether this system would be universally valuable for quantitative prediction of intestinal availability when multiple transporters and/or metabolic enzymes are simultaneously involved in drug absorption. Whether this system can be used for examining clinical drug interactions also remains challenge. For example, AUC_{po} of organic anion transporting polypeptide (OATP) 1A2/OATP2B1 substrate drugs such as fexofenadine and β-blockers (talinolol and nadolol) were reduced by 44–85% after co-administration of grapefruit juice or green tea (Dresser et al., 2002; Schwarz et al., 2005;

Downloaded from dmd.aspetjournals.org at ASPET Journals on April 19, 2024

Misaka et al., 2014). These drug-food interactions were considered to be attributed to the inhibition of OATP2B1/1A2 by food components (Yu et al., 2017), whereas some studies suggested that the change of luminal water volume depending on the osmolality by oral administration of fruit juice indirectly affects intestinal drug absorption (Ichijo et al., 2017; Funai et al., 2019). This system may give us a clue of the mechanism of such drug interactions.

Besides the pharmacokinetic analysis, this system has a potential application as *in vitro* pharmacology model of human intestine. For example, intestinal cholesterol transporter Niemann-Pick C1-like 1 and ileal bile acid transporter are pharmacological targets of ezetimibe (a drug for treatment of hypercholesterolemia) and elobixibat (a drug for treatment of chronic idiopathic constipation), respectively (Yamanashi et al., 2018; Miner PB Jr. 2019). This system could aid future discovery and optimization of drug candidates with gastrointestinal targets/mechanisms of action.

In conclusion, human intestinal spheroid-derived differentiated intestinal epithelial cells could be useful for investigating the impact of intestinal drug-metabolizing enzymes and transporters on the intestinal absorption of substrate drugs in humans.

Downloaded from dmd.aspetjournals.org at ASPET Journals on April 19, 2024

Acknowledgments

The authors thank Drs. Hiroyuki Miyoshi and Makoto Mark Taketo, Kyoto University, for their technical assistance with human intestinal spheroid culture. We also thank Drs. Hiroyuki Nishiyama and Tomoyo Takeuchi, Tsukuba Human Tissue Biobank Center, and Drs. Satoshi Suzuki and Katashi Fukao, Human and Animal Bridging Research Organization, for their kind assistance with establishing the infrastructure to obtain freshly isolated human intestinal sections.

Authorship Contributions

Participated in research design: M, M, K, and O. Conducted experiments: M and M. Performed data analysis: M, M, and K. Wrote or contributed to the writing of the manuscript: M, M, K, and O. Contributed to the provision of human intestinal sections: K, E, S, and O.

Downloaded from dmd.aspetjournals.org at ASPET Journals on April 19, 2024

References

Artursson P, and Karlsson J (1991) Correlation between oral drug absorption in humans and apparent drug permeability coefficients in human intestinal epithelial (Caco-2) cells. *Biochem Biophys Res Commun* **175**:880–885.

Corrò C, Novellasdemunt L, and Li VSW (2020) A brief history of organoids. *Am J Physiol Cell Physiol* **319**:C151–C165.

Dresser GK, Bailey DG, Leake BF, Schwarz UI, Dawson PA, Freeman DJ, and Kim RB (2002) Fruit juices inhibit organic anion transporting polypeptide-mediated drug uptake to decrease the oral availability of fexofenadine. *Clin Pharmacol Ther* **71**:11–20.

Drozdzik M, Gröer C, Penski J, Lapczuk J, Ostrowski M, Lai Y, Prasad B, Unadkat JD, Siegmund W, and Oswald S (2014) Protein abundance of clinically relevant multidrug transporters along the entire length of the human intestine. *Mol Pharm* **11**:3547–3555.

Fenner KS, Troutman MD, Kempshall S, Cook JA, Ware JA, Smith DA, and Lee CA (2009) Drug-drug interactions mediated through P-glycoprotein: clinical relevance and in vitro-in vivo correlation using digoxin as a probe drug. *Clin Pharmacol Ther* **85**:173–181.

Finkbeiner SR, Hill DR, Altheim CH, Dedhia PH, Taylor MJ, Tsai Y-H, Chin AM, Mahe MM, Watson CL, Freeman JJ, Nattiv R, Thomson M, Klein OD, Shroyer NF, Helmrath MA, Teitelbaum DH, Dempsey PJ, and Spence JR (2015) Transcriptome-wide Analysis Reveals Hallmarks of Human Intestine Development and Maturation In Vitro and In Vivo. *Stem Cell Reports*, doi: 10.1016/j.stemcr.2015.04.010.

Fritz A, Busch D, Lapczuk J, Ostrowski M, Drozdzik M, and Oswald S (2019) Expression of clinically relevant drug-metabolizing enzymes along the human intestine and their correlation to drug transporters and nuclear receptors: An intra-subject analysis. *Basic Clin Pharmacol Toxicol* **124**:245–255.

Funai Y, Shirasaka Y, Ishihara M, Takemura M, Ichijo K, Kishimoto H, and Inoue K (2019) Effect of Osmolality on the Pharmacokinetic Interaction between Apple Juice and Atenolol in Rats. *Drug Metab Dispos* **47**:386–391.

Downloaded from dmd.aspetjournals.org at ASPET Journals on April 19, 2024

Greiner B, Eichelbaum M, Fritz P, Kreichgauer HP, von Richter O, Zundler J, and Kroemer HK (1999) The role of intestinal P-glycoprotein in the interaction of digoxin and rifampin. *J Clin Invest* **104**:147–153.

Holtbecker N, Fromm MF, Kroemer HK, Ohnhaus EE, and Heidemann H (1996) The nifedipine-rifampin interaction. Evidence for induction of gut wall metabolism. *Drug Metab Dispos* **24**:1121–1123.

Ichijo K, Oda R, Ishihara M, Okada R, Moteki Y, Funai Y, Horiuchi T, Kishimoto H, Shirasaka Y, and Inoue K (2017) Osmolality of Orally Administered Solutions Influences Luminal Water Volume and Drug Absorption in Intestine. *J Pharm Sci* **106**:2889–2894.

Kabeya T, Mima S, Imakura Y, Miyashita T, Ogura I, Yamada T, Yasujima T, Yuasa H, Iwao T, and Matsunaga T (2020) Pharmacokinetic functions of human induced pluripotent stem cell-derived small intestinal epithelial cells. *Drug Metab Pharmacokinet* **35**:374–382.

Kabeya T, Qiu S, Hibino M, Nagasaki M, Kodama N, Iwao T, and Matsunaga T (2018) Cyclic AMP Signaling Promotes the Differentiation of Human Induced Pluripotent Stem Cells into Intestinal Epithelial Cells. *Drug Metab Dispos* **46**:1411–1419.

Kato M (2008) Intestinal first-pass metabolism of CYP3A4 substrates. *Drug Metab Pharmacokinet* **23**:87–94.

Kawai K, Negoro R, Ichikawa M, Yamashita T, Deguchi S, Harada K, Hirata K, Takayama K, and Mizuguchi H (2020) Establishment of SLC15A1/PEPT1-Knockout Human-Induced Pluripotent Stem Cell Line for Intestinal Drug Absorption Studies. *Mol Ther Methods Clin Dev* **17**:49–57.

Kodama N, Iwao T, Kabeya T, Horikawa T, Niwa T, Kondo Y, Nakamura K, and Matsunaga T (2016) Inhibition of mitogen-activated protein kinase kinase, DNA methyltransferase, and transforming growth factor-β promotes differentiation of human induced pluripotent stem cells into enterocytes. *Drug Metab Pharmacokinet* **31**:193–200.

Kodama N, Iwao T, Katano T, Ohta K, Yuasa H, and Matsunaga T (2016) Characteristic

Downloaded from dmd.aspetjournals.org at ASPET Journals on April 19, 2024

Analysis of Intestinal Transport in Enterocyte-Like Cells Differentiated from Human Induced Pluripotent Stem Cells. *Drug Metab Dispos* **44**:0.

Meran L, Massie I, Campinoti S, Weston AE, Gaifulina R, Tullie L, Faull P, Orford M, Kucharska A, Baulies A, Novellasdemunt L, Angelis N, Hirst E, König J, Tedeschi AM, Pellegata AF, Eli S, Snijders AP, Collinson L, Thapar N, Thomas GMH, Eaton S, Bonfanti P, De Coppi P, and Li VSW (2020) Engineering transplantable jejunal mucosal grafts using patient-derived organoids from children with intestinal failure. *Nat Med* **26**:1593–1601.

Michiba K, Maeda K, Kurimori K, Enomoto T, Shimomura O, Takeuchi T, Nishiyama H, Oda T, and Kusuhara H (2021) Characterization of the Human Intestinal Drug Transport with Ussing Chamber System Incorporating Freshly Isolated Human Jejunum. *Drug Metab Dispos* **49**:84–93.

Middendorp S, Schneeberger K, Wiegerinck CL, Mokry M, Akkerman RDL, van Wijngaarden S, Clevers H, and Nieuwenhuis EES (2014) Adult stem cells in the small intestine are intrinsically programmed with their location-specific function. *Stem Cells* **32**:1083–1091.

Miner PB Jr (2018) Elobixibat, the first-in-class Ileal Bile Acid Transporter inhibitor, for the treatment of Chronic Idiopathic Constipation. *Expert Opin Pharmacother* **19**:1381–1388.

Misaka S, Yatabe J, Müller F, Takano K, Kawabe K, Glaeser H, Yatabe MS, Onoue S, Werba JP, Watanabe H, Yamada S, Fromm MF, and Kimura J (2014) Green tea ingestion greatly reduces plasma concentrations of nadolol in healthy subjects. *Clin Pharmacol Ther* **95**:432–438.

Miyoshi H, and Stappenbeck TS (2013) In vitro expansion and genetic modification of gastrointestinal stem cells in spheroid culture. *Nat Protoc* **8**:2471–2482.

Mizuno N, Niwa T, Yotsumoto Y, and Sugiyama Y (2003) Impact of drug transporter studies on drug discovery and development. *Pharmacol Rev* **55**:425–461.

Müller J, Keiser M, Drozdzik M, and Oswald S (2017) Expression, regulation and function

Downloaded from dmd.aspetjournals.org at ASPET Journals on April 19, 2024

of intestinal drug transporters: an update. *Biol Chem* **398**:175–192.

Nakamura T, Sakaeda T, Ohmoto N, Tamura T, Aoyama N, Shirakawa T, Kamigaki T, Nakamura T, Kim KI, Kim SR, Kuroda Y, Matsuo M, Kasuga M, and Okumura K (2002) Real-time quantitative polymerase chain reaction for MDR1, MRP1, MRP2, and CYP3A-mRNA levels in Caco-2 cell lines, human duodenal enterocytes, normal colorectal tissues, and colorectal adenocarcinomas. *Drug Metab Dispos* **30**:4–6.

Rozehnal V, Nakai D, Hoepner U, Fischer T, Kamiyama E, Takahashi M, Yasuda S, and Mueller J (2012) Human small intestinal and colonic tissue mounted in the Ussing chamber as a tool for characterizing the intestinal absorption of drugs. *Eur J Pharm Sci* **46**:367–373.

Sato T, Vries RG, Snippert HJ, van de Wetering M, Barker N, Stange DE, van Es JH, Abo A, Kujala P, Peters PJ, and Clevers H (2009) Single Lgr5 stem cells build crypt-villus structures in vitro without a mesenchymal niche. *Nature* **459**:262–265.

Schwarz UI, Seemann D, Oertel R, Miehlke S, Kuhlisch E, Fromm MF, Kim RB, Bailey DG, and Kirch W (2005) Grapefruit juice ingestion significantly reduces talinolol bioavailability. *Clin Pharmacol Ther* **77**:291–301.

Seithel A, Karlsson J, Hilgendorf C, Björquist A, and Ungell A-L (2006) Variability in mRNA expression of ABC- and SLC-transporters in human intestinal cells: comparison between human segments and Caco-2 cells. *Eur J Pharm Sci* **28**:291–299.

Sjöberg Å, Lutz M, Tannergren C, Wingolf C, Borde A, and Ungell A-L (2013) Comprehensive study on regional human intestinal permeability and prediction of fraction absorbed of drugs using the Ussing chamber technique. *Eur J Pharm Sci* **48**:166–180.

Sparreboom A, Loos WJ, Burger H, Sissung TM, Verweij J, Figg WD, Nooter K, and Gelderblom H (2005) Effect of ABCG2 genotype on the oral bioavailability of topotecan. *Cancer Biol Ther* **4**:650–658.

Takano J, Maeda K, Bolger MB, and Sugiyama Y (2016) The Prediction of the Relative

Downloaded from dmd.aspetjournals.org at ASPET Journals on April 19, 2024

Importance of CYP3A/P-glycoprotein to the Nonlinear Intestinal Absorption of Drugs by Advanced Compartmental Absorption and Transit Model. *Drug Metab Dispos* **44**:1808–1818.

Urquhart BL, Ware JA, Tirona RG, Ho RH, Leake BF, Schwarz UI, Zaher H, Palandra J, Gregor JC, Dresser GK, and Kim RB (2008) Breast cancer resistance protein (ABCG2) and drug disposition: intestinal expression, polymorphisms and sulfasalazine as an in vivo probe. *Pharmacogenet Genomics* **18**:439–448.

van der Hee B, Loonen LMP, Taverne N, Taverne-Thiele JJ, Smidt H, and Wells JM (2018) Optimized procedures for generating an enhanced, near physiological 2D culture system from porcine intestinal organoids. *Stem Cell Res* **28**:165–171.

VanDussen KL, Marinshaw JM, Shaikh N, Miyoshi H, Moon C, Tarr PI, Ciorba MA, and Stappenbeck TS (2015) Development of an enhanced human gastrointestinal epithelial culture system to facilitate patient-based assays. *Gut* **64**:911–920.

Varma MVS, Obach RS, Rotter C, Miller HR, Chang G, Steyn SJ, El-Kattan A, and Troutman MD (2010) Physicochemical space for optimum oral bioavailability: contribution of human intestinal absorption and first-pass elimination. *J Med Chem* **53**:1098–1108.

Xie F, Ding X, and Zhang Q-Y (2016) An update on the role of intestinal cytochrome P450 enzymes in drug disposition. *Acta Pharm Sin B* **6**:374–383.

Yamanashi Y, Takada T, and Suzuki H (2018) Associations between Lifestyle-Related Diseases and Transporters Involved in Intestinal Absorption and Biliary Excretion of Cholesterol. *Biol Pharm Bull* **41**:1–10.

Yamashita T, Inui T, Yokota J, Kawakami K, Morinaga G, Takatani M, Hirayama D, Nomoto R, Ito K, Cui Y, Ruez S, Harada K, Kishimoto W, Nakase H, and Mizuguchi H (2021) Monolayer platform using human biopsy-derived duodenal organoids for pharmaceutical research. *Mol Ther Methods Clin Dev* **22**:263–278.

Yoshida S, Honjo T, Iino K, Ishibe R, Leo S, Shimada T, Watanabe T, Ishikawa M, Maeda

Downloaded from dmd.aspetjournals.org at ASPET Journals on April 19, 2024

K, Kusuhara H, Shiraki N, and Kume S (2021) Generation of Human-Induced Pluripotent Stem Cell-Derived Functional Enterocyte-Like Cells for Pharmacokinetic Studies. *Stem Cell Reports* **16**:295–308.

Yu J, Zhou Z, Tay-Sontheimer J, Levy RH, and Ragueneau-Majlessi I (2017) Intestinal Drug Interactions Mediated by OATPs: A Systematic Review of Preclinical and Clinical Findings. *J Pharm Sci* **106**:2312–2325.

Zhang W, Yu B-N, He Y-J, Fan L, Li Q, Liu Z-Q, Wang A, Liu Y-L, Tan Z-R, Fen-Jiang, Huang Y-F, and Zhou H-H (2006) Role of BCRP 421C>A polymorphism on rosuvastatin pharmacokinetics in healthy Chinese males. *Clin Chim Acta* **373**:99–103.

Downloaded from dmd.aspetjournals.org at ASPET Journals on April 19, 2024

Footnote

This study was supported by two Grants-in-Aid for Scientific Research (Grant 20H03402 to K.Ma. and T.O. and Grant 20H03401 to H.K.) from the Ministry of Education, Culture, Sports, Science, and Technology in Japan.

The authors declare there are no actual or perceived conflicts of interest with the contents of this article.

Downloaded from dmd.aspetjournals.org at ASPET Journals on April 19, 2024

Figure legends

Fig. 1. Establishment of human intestinal spheroids and generation of 2D cultures from 3D spheroid cultures

(**A**) Images of the human jejunal sample and the procedure for the establishment of human intestinal spheroids from isolated crypts. (**B**) Images of human jejunal spheroids after several passages and the procedure for the generation of 2D cultures from 3D spheroid cultures. (**C**) Timeline for the generation of 2D cultures.

Fig. 2. The relative mRNA expression levels of P-gp, PEPT1, CYP3A4, and SI and transepithelial electrical resistance (TEER) values depending on the culture period.

The mRNA expression levels of (**A**) *ABCB1* (P-gp), (**B**) *SLC15A1* (PEPT1), (**C**) *CYP3A4*, and (**D**) *sucrase-isomaltase* (*SI*) in human jejunal spheroids at 6 days after passage (black column, Day 0) and human jejunal spheroid-derived differentiated intestinal epithelial cells seeded into 24-well plates (gray column; Days 3, 5, 7, 9, 11, and 13) are presented as fold change relative to their expression levels in human jejunal tissue sections. Each bar and error bar represent the mean value and standard deviation (SD), respectively (n = 3). (**E**) TEER values depending on the culture period in human jejunal spheroid-derived differentiated intestinal epithelial cells. Each symbol and error bar represent the mean value and SD, respectively (n = 3).

Fig. 3. Bidirectional transport of P-gp and BCRP substrate drugs in the presence or absence of a cocktail of P-gp/BCRP inhibitors.

Bidirectional transport of (**A**) digoxin and (**B**) fexofenadine (5 μM each; P-gp substrate drugs), (**C**) sulfasalazine and (**D**) rosuvastatin (5 μM each; BCRP substrate drugs), (**E**) antipyrine (1 μM; a passive transcellular transport marker), and (**F**) lucifer yellow (10 μM; a paracellular transport marker) across human jejunal spheroid-derived differentiated intestinal epithelial cells in the presence (open symbol) or absence (closed symbol) of a

Downloaded from dmd.aspetjournals.org at ASPET Journals on April 19, 2024

mixture of PSC833 (5 μM; a P-gp inhibitor) and Ko143 (5 μM; a BCRP inhibitor). Square and triangle symbols represent the transport in the apical-to-basolateral direction (A to B) and in the basolateral-to-apical direction (B to A), respectively. Each symbol and error bar represent the mean value and SD, respectively (n = 3). The apparent permeability coefficient (P_{app}) of (**G**) digoxin, (**H**) fexofenadine, (**I**) sulfasalazine, (**J**) rosuvastatin, (**K**) antipyrine, and (**L**) lucifer yellow across human jejunal spheroid-derived differentiated intestinal epithelial cells in the presence (open column) or absence (closed column) of a mixture of PSC833 and Ko143. Each bar and error bar represent the mean value and SD, respectively (n = 3). * indicates significant difference in the transport or P_{app} in the presence of a mixture of PSC833 and Ko143 compared with that of control (*$p < 0.05$, **$p < 0.01$). # indicates significant difference in the transport or P_{app} in the basolateral-to-apical direction compared with that in the apical-to-basolateral direction (#$p < 0.05$, ##$p < 0.01$).

Fig. 4. Apical-to-basolateral transport of cefadroxil in the presence or absence of PEPT1 inhibitor (glycylsarcosine; Gly-Sar).

Apical-to-basolateral (A to B) transport of (A) cefadroxil (10 μM; a PEPT1 substrate), (B) antipyrine (1 μM; a passive transcellular transport marker), and (C) lucifer yellow (10 μM; a paracellular transport marker) across human jejunal spheroid-derived differentiated intestinal epithelial cells in the presence (open square) or absence (closed square) of Gly-Sar (10 mM; a PEPT1 inhibitor). Each symbol and error bar represent the mean value and SD, respectively (n = 3). The P_{app} values in the apical-to-basolateral direction of (D) cefadroxil, (E) antipyrine, and (F) lucifer yellow across human jejunal spheroid-derived differentiated intestinal epithelial cells in the presence (open column) or absence (closed column) of Gly-Sar. Each bar and error bar represent the mean value and SD, respectively (n = 3). *$p < 0.05$, **$p < 0.01$.

Fig. 5. Metabolism of CYP3A4/5, CYP2C9, UGT1As, and CES2 substrate drugs in the

Downloaded from dmd.aspetjournals.org at ASPET Journals on April 19, 2024

presence or absence of the corresponding inhibitors.

Metabolic activities of (A) CYP3A4/5 (5 μM midazolam; midazolam 1′-hydroxylation), (B) CYP2C9 (10 μM diclofenac; diclofenac 4′-hydroxylation), (C) UGT1As (5 μM raloxifene; raloxifene 4′-glucuronidation), and (D) CES2 (50 μM irinotecan; irinotecan hydrolysis) in human jejunal spheroid-derived differentiated intestinal epithelial cells in the presence (open column) or absence (closed column) of ketoconazole (10 μM; a CYP3A4/5 inhibitor), sulfaphenazole (50 μM; a CYP2C9 inhibitor), zafirlukast (50 μM; an UGT inhibitor), or loperamide (20 μM; a CES inhibitor). Each bar and error bar represent the mean value and SD, respectively (n = 3). *$p < 0.05$, **$p < 0.01$.

Fig. 6. Apical-to-basolateral transport of CYP3A substrate drugs in the presence or absence of a CYP3A inhibitor (ketoconazole) and/or CYP3A inducer (1,25-$(OH)_2D_3$).

Apical-to-basolateral (A to B) transport of (**A**) midazolam, (**B**) triazolam, (**C**) alprazolam, (**D**) felodipine, and (**E**) nifedipine (1 μM each; CYP3A substrates) across human jejunal spheroid-derived differentiated intestinal epithelial cells in the presence (open symbol) or absence (closed symbol) of ketoconazole (10 μM; a CYP3A inhibitor) with (circle symbol) or without (square symbol) 1,25-$(OH)_2D_3$ (10 nM for 96 h; a CYP3A inducer). Each symbol and error bar represent the mean value and SD, respectively (n = 3). The P_{app} values of (**F**) midazolam, (**J**) triazolam, (**H**) alprazolam, (**I**) felodipine, and (**J**) nifedipine in the apical-to-basolateral direction across human jejunal spheroid-derived differentiated intestinal epithelial cells in the presence (open column) or absence (closed column) of ketoconazole with or without 1,25-$(OH)_2D_3$. Each bar and error bar represent the mean value and SD, respectively (n = 3). The production clearance of (**K**) 1′-hydroxy midazolam, (**L**) α-hydroxy triazolam, (**M**) α-hydroxy alprazolam, (**N**) dehydro-felodipine, and (**O**) dehydro-nifedipine (metabolites of CYP3A substrates) in human jejunal spheroid-derived differentiated intestinal epithelial cells in the presence (open column) or absence (closed column) of ketoconazole with or without 1,25-$(OH)_2D_3$. Each bar and error bar represent the mean

Downloaded from dmd.aspetjournals.org at ASPET Journals on April 19, 2024

value and SD, respectively (n = 3). * indicates significant difference in the apical-to-basolateral transport, P_{app} in the apical-to-basolateral direction, or production clearance of metabolites in the presence of ketoconazole compared with that of control (*p < 0.05, **p < 0.01). # indicates significant difference in the apical-to-basolateral transport, P_{app} in the apical-to-basolateral direction, or production clearance of metabolites with 1,25-$(OH)_2D_3$ compared with that of control (#p < 0.05, ##p < 0.01). ND; not detected.

Fig. 7. Correlation between the estimated and *in vivo* human intestinal availability (Fg) values of CYP3A substrate drugs.

Comparisons of the estimated Fg values of midazolam, triazolam, alprazolam, felodipine, and nifedipine calculated using Eqs (3)–(6) in the presence (open circle) or absence (closed circle) of 1,25-$(OH)_2D_3$ (a CYP3A inducer) and their corresponding *in vivo* human Fg values. The solid line represents an identity line. Each symbol and error bar represent the mean value and SD, respectively (n = 3).

Downloaded from dmd.aspetjournals.org at ASPET Journals on April 19, 2024

Table 1. Summary of estimated intestinal availability (Fg) values for CYP3A substrates

Data are presented as the mean ± standard deviation (n = 3).

1,25$(OH)_2D_3$, 1α, 25-dihydroxyvitamin D_3; CL_{AtoB}, transcellular transport clearance in the apical-to-basolateral direction; KCZ, ketoconazole

a: Varma et al. (2010)

Compound	CL_{AtoB} (μL/120 min)				Estimated Fg value		*In vivo* human Fg value[a]
	Control		+1,25$(OH)_2D_3$				
	Control	+KCZ	Control	+KCZ	Control	+1,25$(OH)_2D_3$	
Felodipine	5.18 ± 0.78	10.1 ± 0.2	2.71 ± 0.62	7.81 ± 1.51	0.35 ± 0.08	0.25 ± 0.14	0.35
Midazolam	73.1 ± 4.7	101 ± 5	50.4 ± 4.3	96.6 ± 4.8	0.58 ± 0.10	0.36 ± 0.05	0.55
Nifedipine	87.6 ± 5.5	104 ± 7	54.9 ± 4.7	95.9 ± 6.3	0.76 ± 0.19	0.41 ± 0.09	0.73
Triazolam	91.3 ± 5.2	97.6 ± 5.7	82.5 ± 5.5	96.6 ± 6.3	0.91 ± 0.20	0.76 ± 0.12	0.74
Alprazolam	85.6 ± 4.1	101 ± 6	79.6 ± 5.7	97.1 ± 5.2	0.75 ± 0.14	0.71 ± 0.12	0.98

Downloaded from dmd.aspetjournals.org at ASPET Journals on April 19, 2024

Fig.1

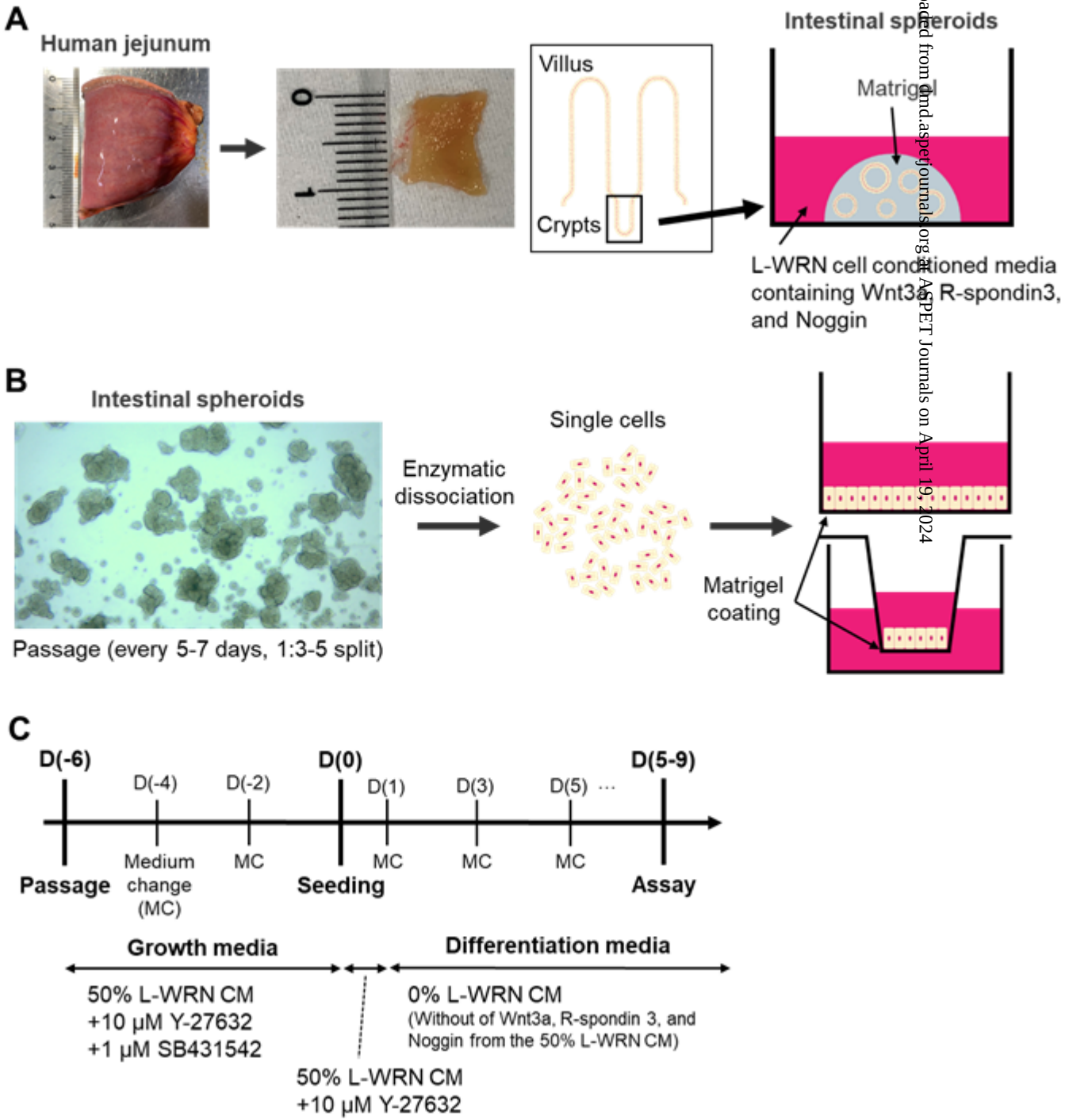

Downloaded from dmd.aspetjournals.org at ASPET Journals on April 19, 2024

Fig.2

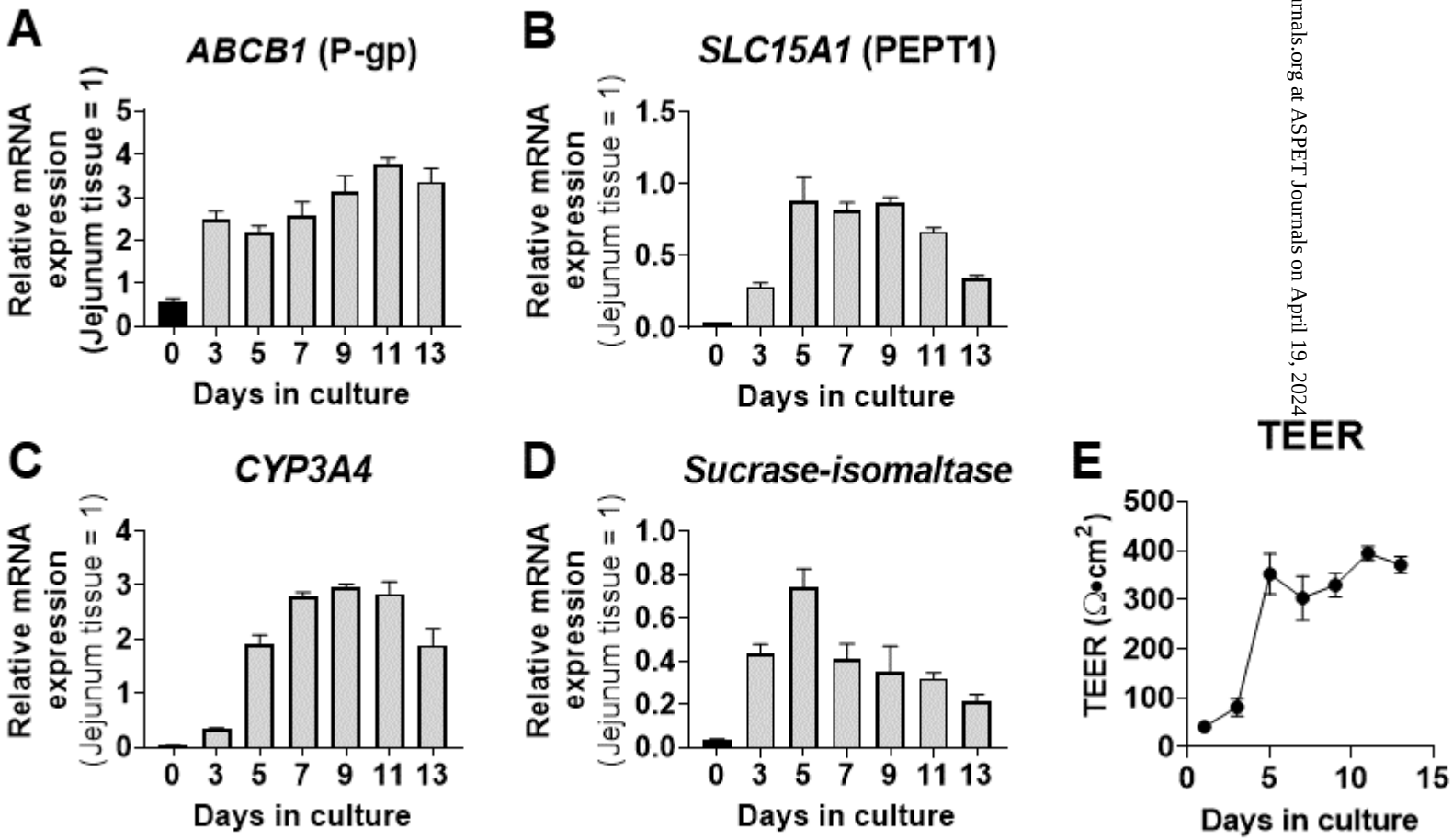

Downloaded from dmd.aspetjournals.org at ASPET Journals on April 19, 2024

Fig.3

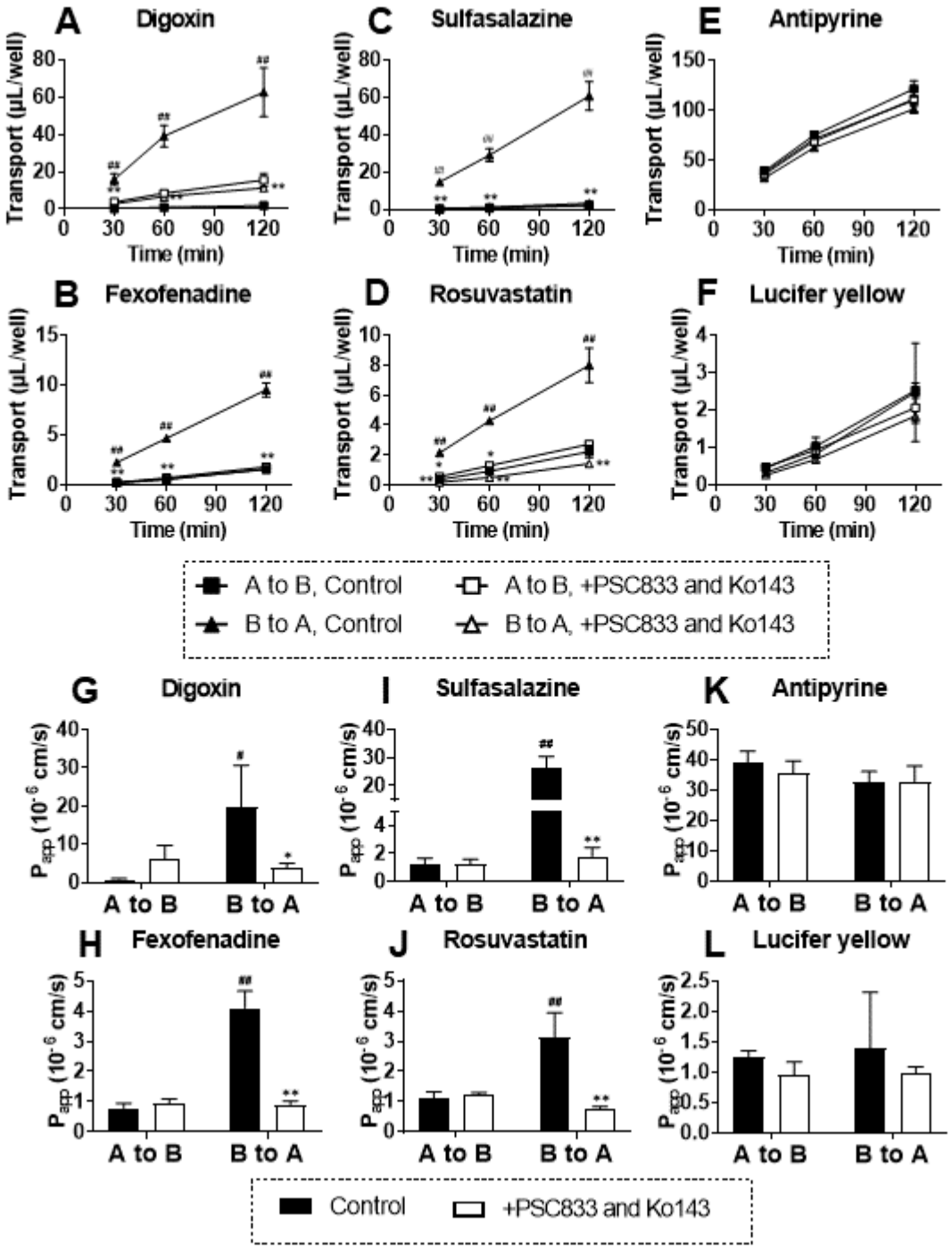

Downloaded from dmd.aspetjournals.org at ASPET Journals on April 19, 2024

Fig.4

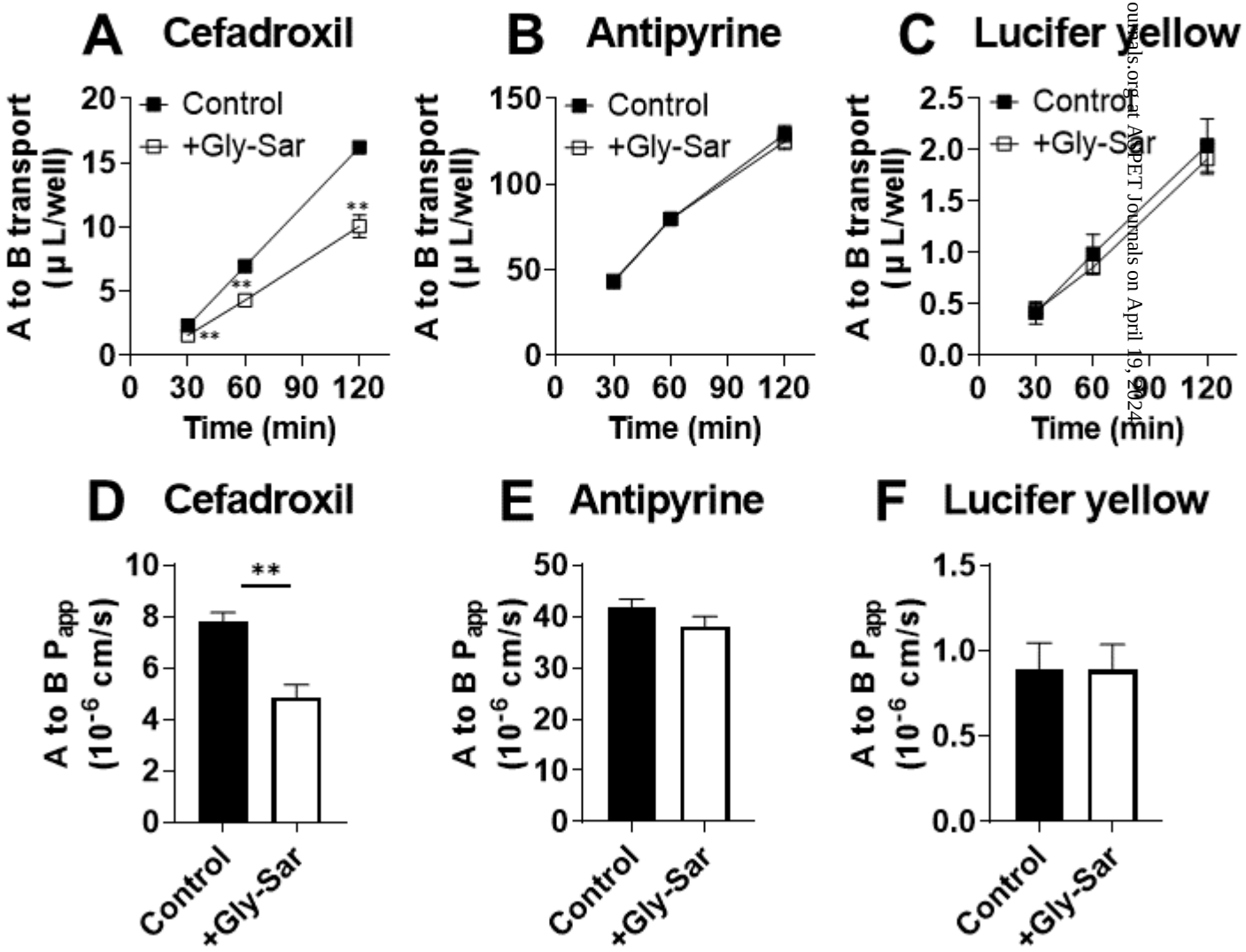

Downloaded from dmd.aspetjournals.org at ASPET Journals on April 19, 2024

Fig.5

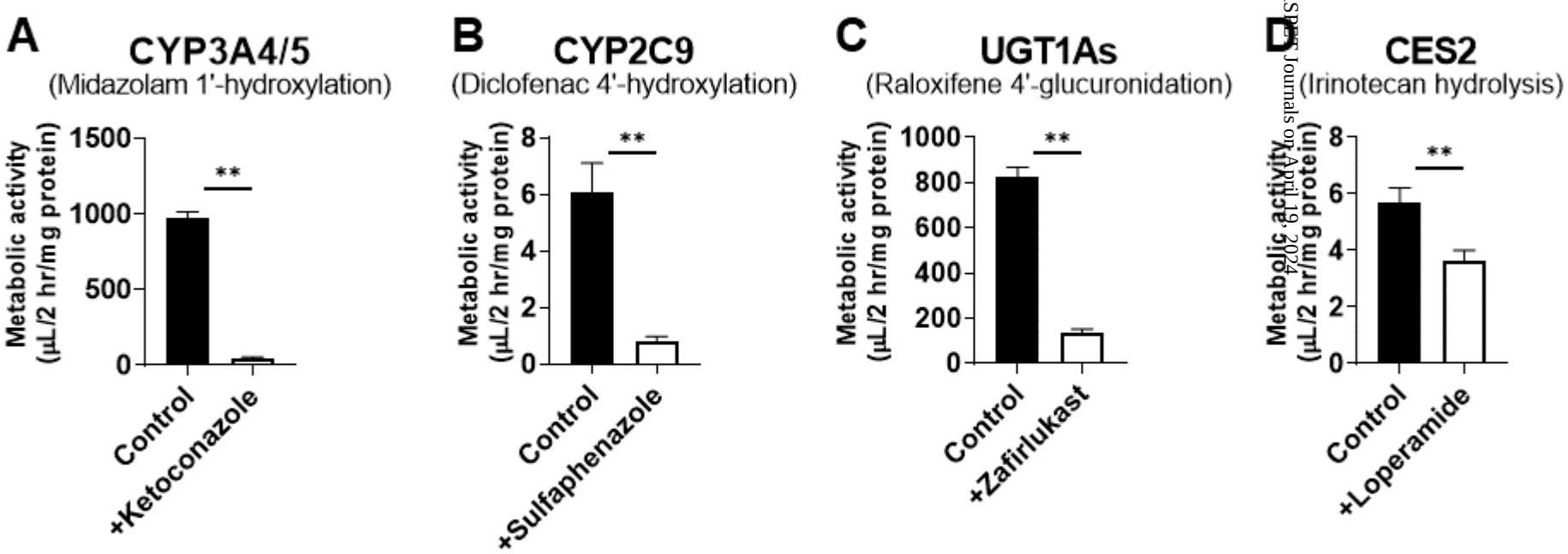

Downloaded from dmd.aspetjournals.org at ASPET Journals on April 19, 2024

Fig.6

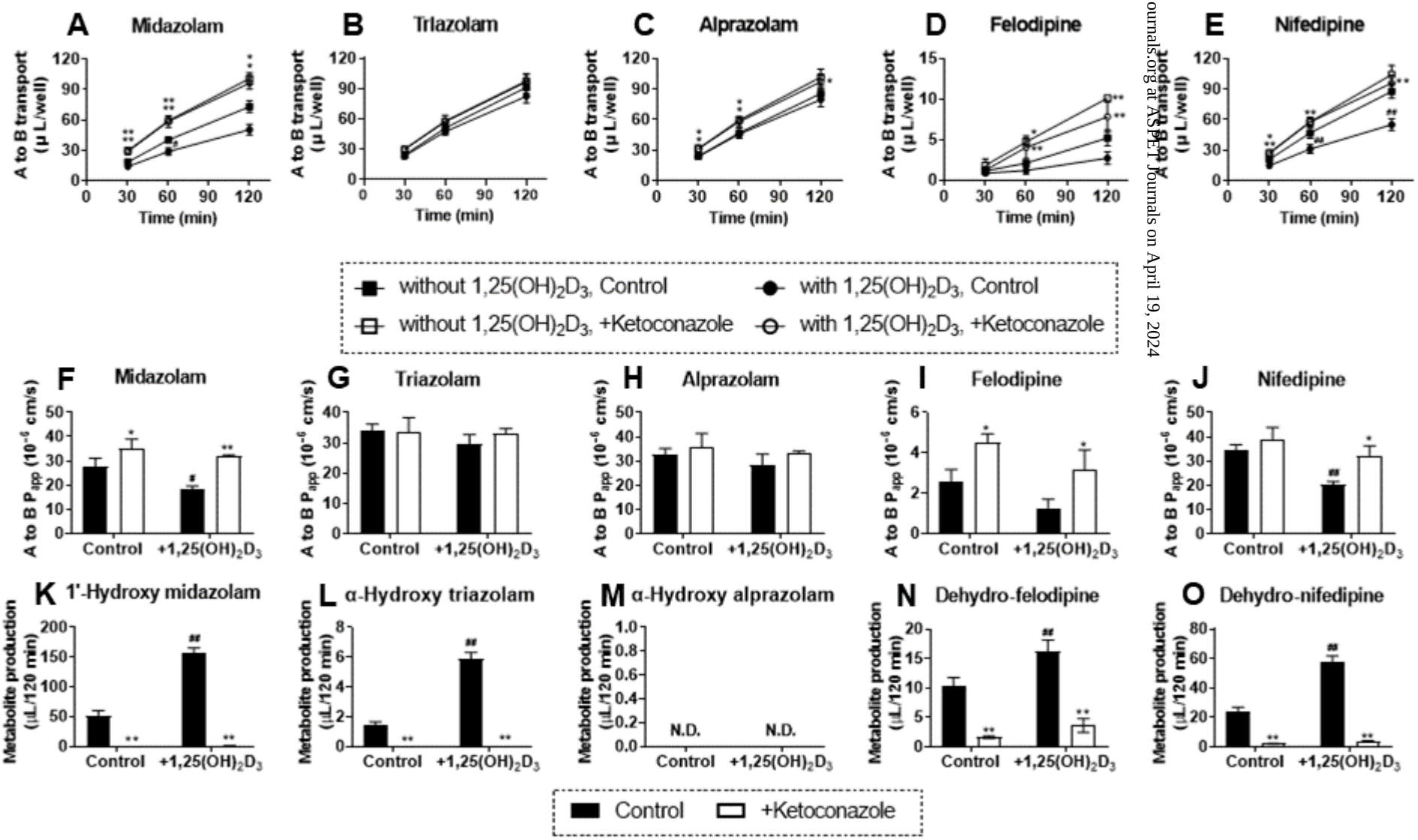

Downloaded from dmd.aspetjournals.org at ASPET Journals on April 19, 2024

Fig.7

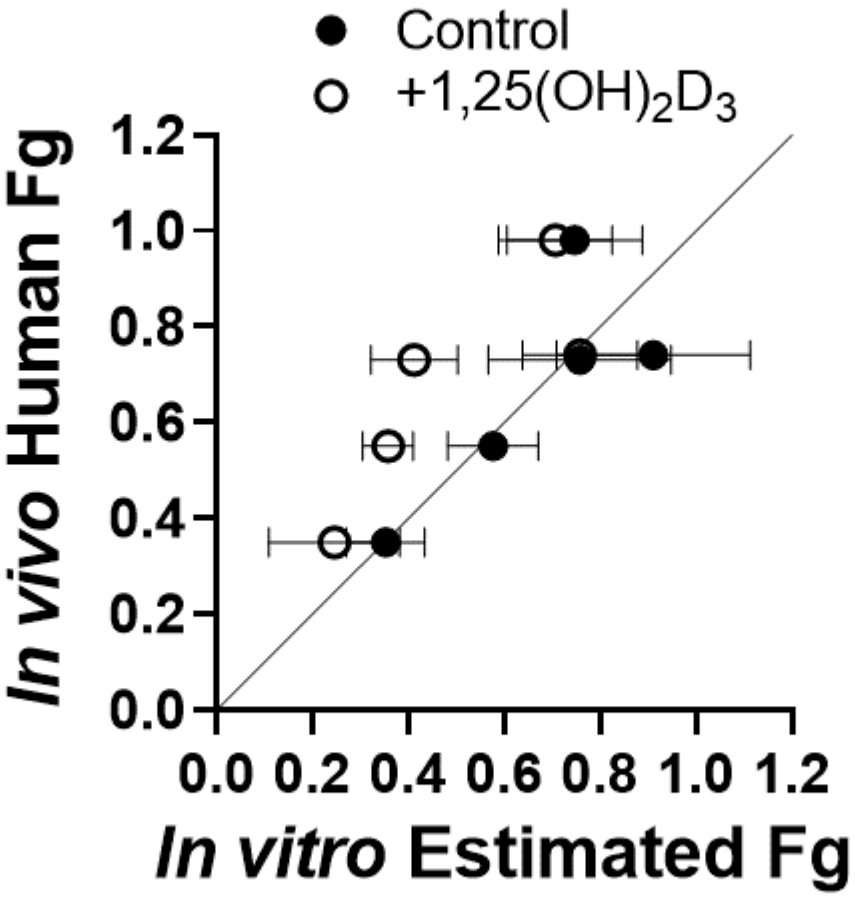

Downloaded from dmd.aspetjournals.org at ASPET Journals on April 19, 2024

Supplementary information

Article title

Usefulness of human jejunal spheroid-derived differentiated intestinal epithelial cells for the prediction of intestinal drug absorption in humans

Authors

Kazuyoshi Michiba, Kazuya Maeda, Osamu Shimomura, Yoshihiro Miyazaki, Shinji Hashimoto, Tatsuya Oda and Hiroyuki Kusuhara

Journal title

Drug metabolism and disposition

Manuscript number

DMD-AR-2021-000796

Supplementary methods

Data analysis

The intestinal availability (Fg) of CYP3A substrates was calculated from the following the equation:

$$Fg = \frac{Parent_{\,(Basolateral)}}{Parent_{\,(Basolateral)} + Metabolite_{\,(Apical\,+Intracellular\,+Basolateral)}} \cdots (7)$$

where Parent $_{(Basolateral)}$ and Metabolite $_{(Apical + Intracellular + Basolateral)}$ represent the total amount of parent drugs (midazolam, triazolam, alprazolam, felodipine and nifedipine) transported to the basolateral compartment after 120 min incubation and the total amount of metabolites (1'-hydroxy midazolam, α-hydroxy triazolam, α-hydroxy alprazolam, dehydro-felodipine and dehydro-nifedipine) appeared in the apical compartment, cells and the basolateral compartment after 120 min incubation.

Supplementary figures and tables

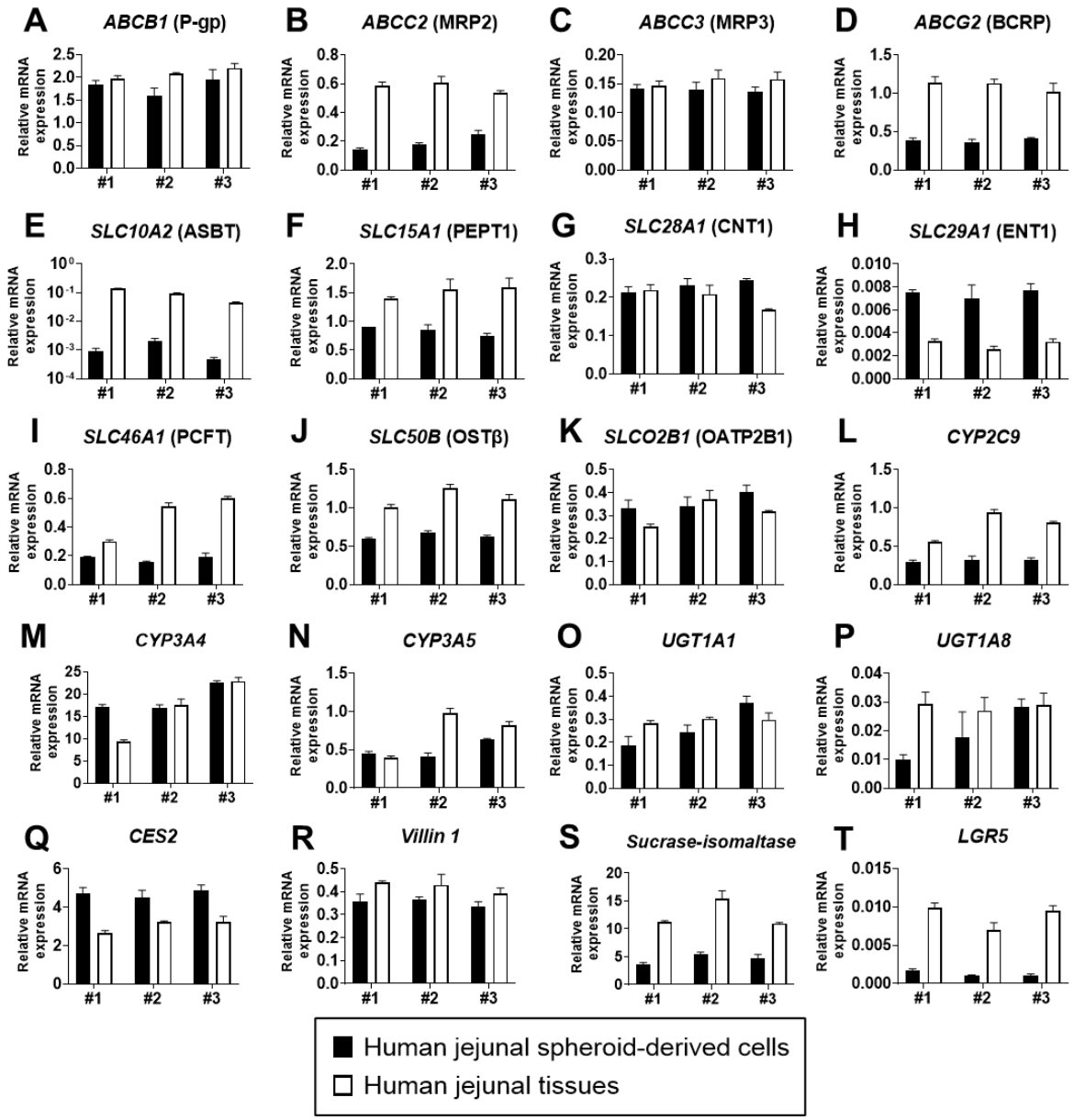

Supplementary Figure 1. The relative mRNA expression levels of intestinal drug transporters and drug-metabolizing enzymes in human jejunal spheroid-derived cells and human jejunal tissue sections originating from 3 different subject (#1–#3).

The mRNA expression levels of (**A**) *ABCB1* (P-gp), (**B**) *ABCC2* (MRP2), (**C**) *ABCC3* (MRP3), (**D**) *ABCG2* (BCRP), (**E**) *SLC10A2* (ASBT), (**F**) *SLC15A1* (PEPT1), (**G**) *SLC28A1* (CNT1), (**H**) *SLC29A1* (ENT1), (**I**) *SLC46A1* (PCFT), (**J**) *SLC50B* (OSTβ), (**K**) *SLCO2B* 1 (OATP2B1),

(**L**) *CYP2C9*, (**M**) *CYP3A4*, (**N**) *CYP3A5*, (**O**) *UGT1A1*, (**P**) *UGT1A8*, (**Q**) *CES2*, (**R**) *Villin 1* (a brush border marker), (**S**) *Sucrase-isomaltase* (a matured enterocyte marker), and (**T**) *LGR5* (a stem cell marker) in human jejunal spheroid-derived differentiated intestinal epithelial cells at 5 days after seeding (closed column) and human jejunal tissue sections (open column) originating from three independent subjects (#1–#3). The geometrical mean values of the mRNA expression levels of housekeeping genes (*GAPDH,* β-actin, and HPRT) were taken as 1.0. Each bar and error bar represent the mean value and SD, respectively (n = 3).

ASBT, apical sodium-dependent bile acid transporter; CNT, concentrative nucleoside transporter; ENT, equilibrative nucleoside transporter; GAPDH, glyceraldehyde-3-phosphate dehydrogenase; HPRT, hypoxanthine phosphoribosyltransferase; LGR5, luecine-rich orphan G-protein-coupled receptor; MRP, multidrug resistance protein; OATP, organic anion transporting polypeptide; OST, organic solute transporter; PCFT, proton-coupled folate transporter

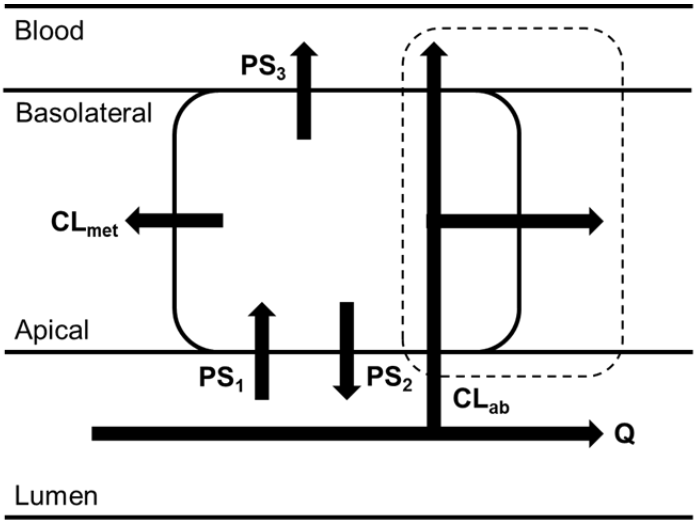

$$F_a = \frac{CL_{ab}}{Q + CL_{ab}} \qquad CL_{ab} = PS_1 \frac{PS_3 + CL_{met}}{PS_2 + PS_3 + CL_{met}}$$

$$F_g = \frac{PS_3}{PS_3 + CL_{met}}$$

$$CL_{A\ to\ B} = PS_1 \frac{PS_3}{PS_2 + PS_3 + CL_{met}} = CL_{ab} F_g$$

$$F_a F_g = \frac{CL_{ab}}{Q + CL_{ab}} \frac{PS_3}{PS_3 + CL_{met}}$$

Supplementary Figure 2. Simple mathematical modeling of intestinal absorption of drugs.

Fa, Fg and FaFg represent the fraction of oral drugs that enters gut wall, intestinal availability and the product of Fa and Fg, respectively. Q represents the apparent flow rate of intestinal contents along the intestinal tract. CL_{ab} represents the apparent absorption clearance, while $CL_{A\ to\ B}$ represents the permeation clearance in the apical-to-basolateral direction. PS_1, PS_2, PS_3 and CL_{met} represent the apical-to-cell passive permeation clearance, cell-to-apical passive permeation clearance, cell-to-basolateral passive permeation clearance and metabolic clearance mediated by CYP3A, respectively.

$$F_a F_g = F_g \left(1 - \frac{F_g Q}{CL_{A\ to\ B} + F_g Q}\right)$$

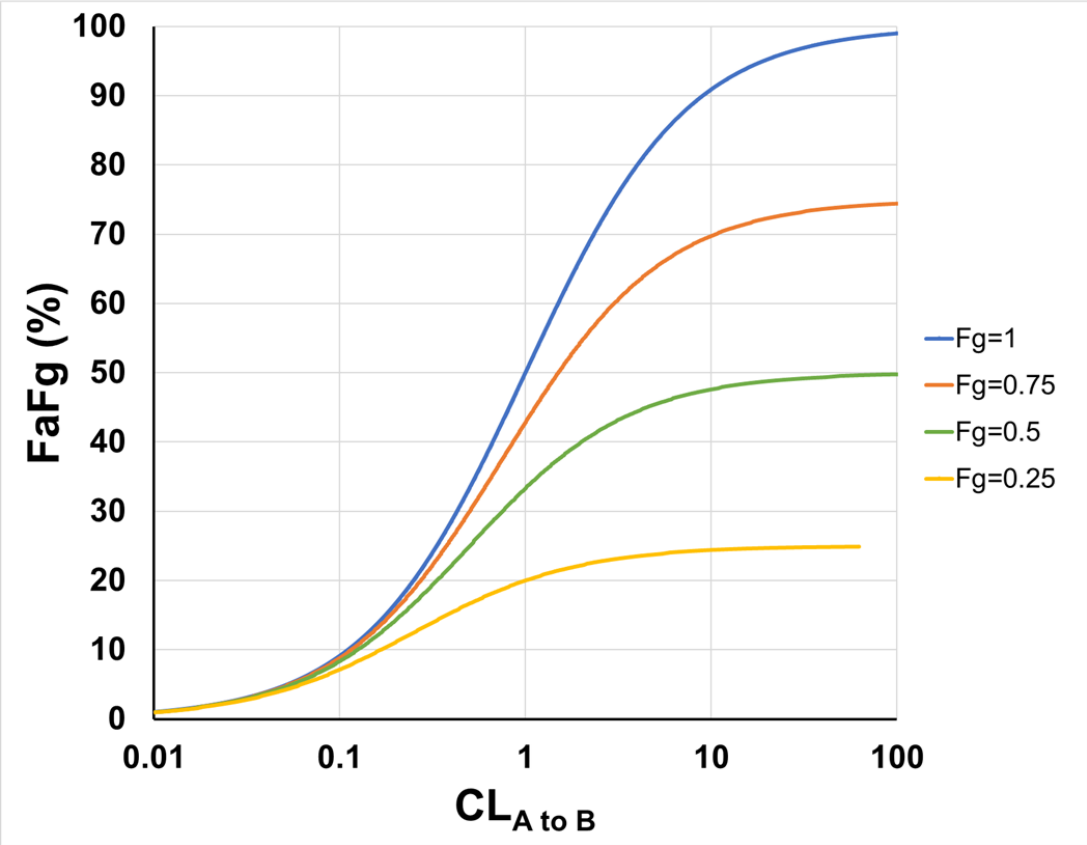

Supplementary Figure 3. Theoretical consideration of the relationship between $CL_{A\ to\ B}$ and FaFg.

Theoretical curves to relate FaFg with $CL_{A\ to\ B}$ were shown when Fg takes 0.25, 0.5, 0.75, and 1.0. Theoretical curves were drawn based on the following the equation (Q was arbitrary set at 1 for simplicity):

$$FaFg = Fg\left(1 - \frac{FgQ}{CL_{A\ to\ B} + FgQ}\right) = Fg(1 - \frac{Fg}{CL_{A\ to\ B} + Fg}) \cdots (8)$$

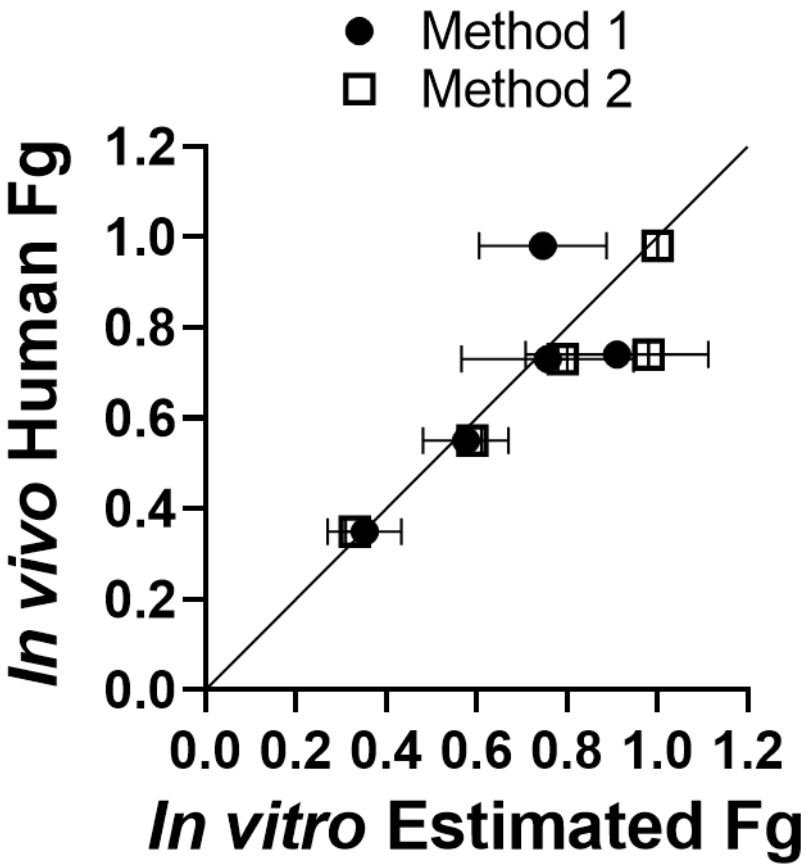

Supplementary Figure 4. Correlation between in vitro estimated Fg values and in vivo human Fg values of CYP3A substrate drugs based on the two different estimation methods.

Comparison of in vitro estimated Fg values of midazolam, triazolam, alprazolam, felodipine and nifedipine calculated with Method 1 (Eq. (6); closed circle) or Method 2 (Eq. (7); open square) and their in vivo human Fg values. The solid line represents the identity line. Each symbol and error bar represent the mean value and SD, respectively (n = 3).

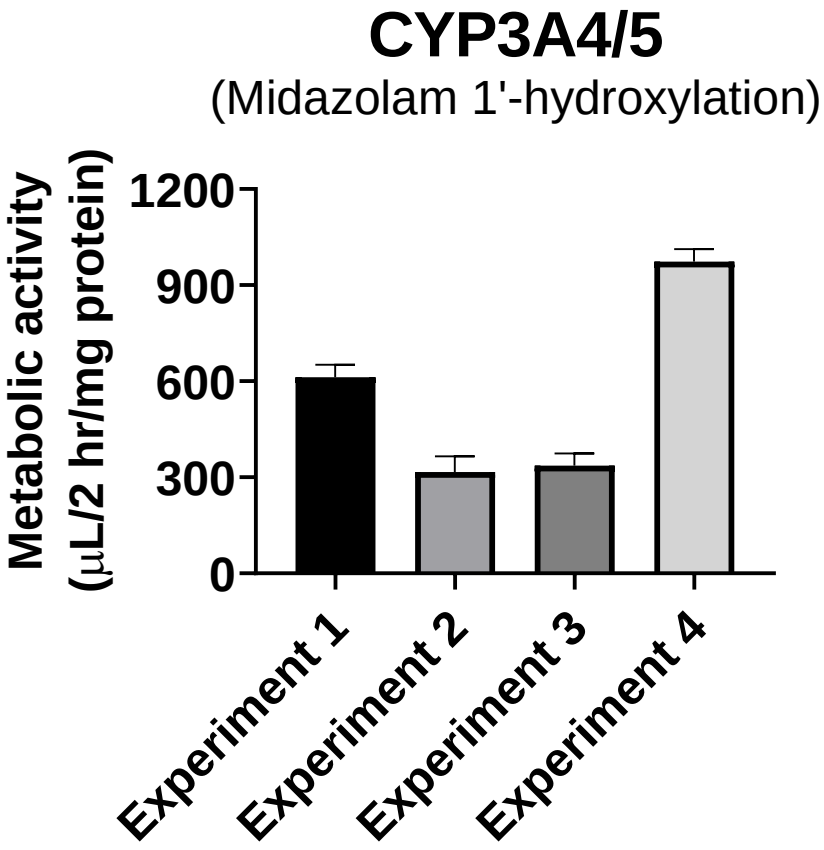

Supplementary Figure 5. Comparison of the metabolic activity mediated by CYP3A4/5 in the four independent experiments.

Metabolic activity of CYP3A4/5 (midazolam 1’-hydroxylation) in human jejunal spheroid-derived differentiated intestinal epithelial cells derived from the same donor was quantified in the four independent experiments. Each bar and error bar represent the mean value and SD, respectively (n = 3).

Supplementary Table 1. Source of chemicals used in this study.

Compound	Purchase source
Digoxin	Merck (Darmstadt, Germany)
Digoxin-d3	Toronto Research Chemicals (North York, Canada)
Fexofenadine	Toronto Research Chemicals (North York, Canada)
Fexofenadine-d10	Toronto Research Chemicals (North York, Canada)
Sulfasalazine	Merck (Darmstadt, Germany)
Sulfasalazine-d4	Toronto Research Chemicals (North York, Canada)
Rosuvastatin	Fujifilm Wako Pure Chemical (Osaka, Japan)
Rosuvastatin-d6	Toronto Research Chemicals (North York, Canada)
Valspodar (PSC833)	Merck (Darmstadt, Germany)
Ko143	ChemScene LLC (Monmouth Junction, NJ)
Cefadroxil	Merck (Darmstadt, Germany)
Cefixime	Fujifilm Wako Pure Chemical (Osaka, Japan)
Glycylsarcosine	Merck (Darmstadt, Germany)
Antipyrine	Fujifilm Wako Pure Chemical (Osaka, Japan)
Talinolol	Toronto Research Chemicals (North York, Canada)
Lucifer yellow	Fujifilm Wako Pure Chemical (Osaka, Japan)
Midazolam	Fujifilm Wako Pure Chemical (Osaka, Japan)
1'-Hydroxy midazolam	Cayman Chemical (Michigan, USA)
Midazolam-d4	Merck (Darmstadt, Germany)
Triazolam	Fujifilm Wako Pure Chemical (Osaka, Japan)
α-Hydroxy triazolam	Merck (Darmstadt, Germany)
Alprazolam	Fujifilm Wako Pure Chemical (Osaka, Japan)
α-Hydroxy alprazolam	Cayman Chemical (Michigan, USA)
Felodipine	Tokyo Chemical Industry (Tokyo, Japan)
Dehydro felodipine	Toronto Research Chemicals (North York, Canada)
Nifedipine	Fujifilm Wako Pure Chemical (Osaka, Japan)
Dehydro nifedipine	Toronto Research Chemicals (North York, Canada)
Nifedipine-d6	Toronto Research Chemicals (North York, Canada)
Ketoconazole	Fujifilm Wako Pure Chemical (Osaka, Japan)
Diclofenac	Fujifilm Wako Pure Chemical (Osaka, Japan)
4-Hydroxy diclofenac	Toronto Research Chemicals (North York, Canada)
Diclofenac-d4	Toronto Research Chemicals (North York, Canada)
Sulfaphenazole	Merck (Darmstadt, Germany)
Raloxifene	Toronto Research Chemicals (North York, Canada)
Raloxifene-4-glucuronide	Toronto Research Chemicals (North York, Canada)
Raloxifene-6-glucuronide	Toronto Research Chemicals (North York, Canada)

Raloxifene-d4	Toronto Research Chemicals (North York, Canada)
Zafirlukast	Tokyo Chemical Industry (Tokyo, Japan)
Irinotecan	Fujifilm Wako Pure Chemical (Osaka, Japan)
SN-38	Toronto Research Chemicals (North York, Canada)
Camptothecin	Fujifilm Wako Pure Chemical (Osaka, Japan)
Loperamide	Fujifilm Wako Pure Chemical (Osaka, Japan)

Supplementary Table 2. Sequences of primers for mRNA quantification.

Gene Name	Sense (5'→3')	Antisense (5'→3')
ABCB1 (P-gp)	CCCATCATTGCAATAGCAGG	TGTTCAAACTTCTGCTCCTGA
ABCC2 (MRP2)	TCTCTCGATACTCTGTGGCAC	CTGGAATCCGTAGGAGATGAAGA
ABCC3 (MRP3)	CACCAACTCAGTCAAACGTGC	GCAAGACCATGAAAGCGACTC
ABCG2 (BCRP)	AGATGGGTTTCCAAGCGTTCAT	CCAGTCCCAGTACGACTGTGACA
CES2	GCGGACTCCATGTTTGTGAT	GGCTGATGCTGGAACTCGTA
CYP2C9	GACATGAACAACCCTCAGGACTTT	TGCTTGTCGTCTCTGTCCCA
CYP3A4	CCTTACATATACACACCCTTTGGAAG	TGGTTGAAGAAGTCCTCCTAAGCT
CYP3A5	CCTTACATATACACACCCTTTGGAAC	GTTGAAGAAGTCCTTGCGTGTC
GAPDH	GGAGCGAGATCCCTCCAAAAT	GGCTGTTGTCATACTTCTCATGG
HPRT	CTTTGCTTTCCTTGGTCAGG	TCAAGGGCATATCCTACAACA
LGR5	CCTTCATAAGAAAGATGCTGGAAT	GTTTAATGGGGGAAATGTACAGAG
SLC10A2 (ASBT)	ATGCAGAACACGCAGCTATG	GCTCCGTTCCATTTTCTTTG
SLC15A1 (PEPT1)	CACCTCCTTGAAGAAGATGGCA	GGGAAGACTGGAAGAGTTTTATCG
SLC28A2 (CNT2)	TACATTGAGGGCAGGCTCAGCG	CATGGGGGCTTTCCTGCCATTG
SLC29A1 (ENT1)	GCTGGGTCTGACCGTTCTAT	AAGGCAGTAACGTGGCAACT
SLC46A1 (PCFT)	TTGCCTTTGCCACTATCACG	ACCAGCTTGGAGAGTTTAGCC
SLC51B (OSTβ)	GGGGCTAAGGGGTCTAAGG	CAGGGCAAGGATGGAATGA
SLCO2B1 (OATP2B1)	CTTCATCTCGGAGCCATACC	GCTTGAGCAGTTGCCATTG
Sucrase-isomaltase	CTGCATTTGAAAGAGGACAGC	ACTCTGCTGTGGAAGTCCTGA
UGT1A1	CCTTGCCTCAGAATTCCTTC	ATTGATCCCAAAGAGAAAACCAC
UGT1A8	GGTCTTCGCCAGGGGAATAG	ATTGATCCCAAAGAGAAAACCAC
Villin 1	ACTACTGGATTGGCCAGGACT	TGGACGTCATAGGAGTTGGTC
β-actin	GGACTTCGAGCAAGAGATGG	AAGGAAGGCTGGAAGAGTGC

Supplementary Table 3. Analytical conditions for quantification of test compounds with LC–MS/MS.

Compounds	Column	Mobile phase	Gradient condition (B concentration %)	Flow rate (mL/min)	Retention time (min)
Digoxin	Atlantis T3 C18 (3 μm, 2.1 mm × 50 mm; Waters)	A: 0.1%FA in distilled water B: 0.1%FA in acetonitrile	0–0.5 min: 5% 0.5–4 min: 5%–95% 4–5 min: 95% 5–5.01 min: 95%–5% 5.01–6 min: 5%	0.4	3.09
Digoxin-d3					3.09
Fexofenadine					3.00
Fexofenadine-d10					3.00
Sulfasalazine					3.26
Sulfasalazine-d4					3.26
Rosuvastatin					3.47
Rosuvastatin-d6					3.47
Cefadroxil					1.90
Cefixime					2.17
Antipyrine					2.49
Talinolol					2.72
Midazolam					2.78
1'-Hydroxy midazolam					3.32
Midazolam-d4					3.28
Triazolam					2.78
α-Hydroxy triazolam					3.22
Alprazolam					3.22

α-Hydroxy alprazolam				2.78
Felodipine				4.29
Dehydro-felodipine				3.66
Nifedipine				4.27
Dehydro-nifedipine				3.63
Nifedipine-d6				3.66
Diclofenac				4.02
4'-hydroxy diclofenac				3.55
Diclofenac-d4				4.02
Irinotecan				2.73
SN-38				3.12
Camptothecin				3.21
Raloxifene		0-0.5 min: 5% 0.5-4.5 min: 5%-50% 4.5-5.5 min: 50%-95% 5.5-6.5 min: 95% 6.5-6.51 min: 95%-5% 6.51-7.5 min: 5%	0.4	4.02
Raloxifene-4'-glucuronide				3.59
Raloxifene-6-glucuronide				3.37
Raloxifene-d4				4.02

Supplementary Table 4. MRM conditions for quantification of test compounds with LC–MS/MS.

DP; declustering potential, CE; collision energy, CXP; collision cell exit potential.

Compounds	Ion mode	Q1 Mass (Da)	Q3 Mass (Da)	DP (V)	CE (V)	CXP (V)	Internal standard	Linear range
Digoxin	positive	781.4	651.4	71	11	20	Digoxin-d3	0.3 nM to 100 nM
Digoxin-d3	positive	784.4	651.4	71	11	20	—	—
Fexofenadine	positive	502.4	466.0	70	40	35	Fexofenadine-d10	0.003 nM to 10 nM
Fexofenadine-d10	positive	512.4	476.0	70	40	35	—	—
Sulfasalazine	negative	396.9	196.9	–45	–32	–23	Sulfasalazine-d4	0.03 nM to 100 nM
Sulfasalazine-d4	negative	400.9	196.9	–45	–32	–23	—	—
Rosuvastatin	positive	482.1	258.1	71	30	28	Rosuvastatin-d6	0.3 nM to 100 nM
Rosuvastatin-d6	positive	488.1	264.1	71	30	28	—	—
Cefadroxil	positive	363.9	208.0	46	13	26	Cefixime	0.1 nM to 300 nM
Cefixime	positive	454.0	285.1	101	21	32	—	—
Antipyrine	positive	189.3	55.9	151	49	12	Talinolol	0.1 nM to 30 nM
Talinolol	positive	364.9	309.2	76	23	18	—	—
Midazolam	positive	326.9	292.0	36	37	26	Midazolam-d4	0.1 nM to 100 nM
1-Hydroxy midazolam	positive	342.1	324.0	60	30	28	Midazolam-d4	0.3 nM to 100 nM
Midazolam-d4	positive	330.9	296.0	36	37	26	—	—
Triazolam	positive	343.1	308.1	141	37	26	Midazolam-d4	0.01 nM to 100 nM
α-Hydroxy triazolam	positive	359.1	330.9	131	37	34	Midazolam-d4	0.1 nM to 300 nM
Alprazolam	positive	309.1	281.1	111	35	26	Midazolam-d4	0.1 nM to 300 nM

α-Hydroxy alprazolam	positive	325.1	297.1	161	33	34	Midazolam-d4	0.01 nM to 100 nM
Felodipine	positive	384.3	338.0	81	9	32	Nifedipine-d6	0.1 nM to 300 nM
Dehydro-felodipine	positive	382.2	287.1	136	49	32	Nifedipine-d6	0.01 nM to 100 nM
Nifedipine	positive	347.2	315.0	71	9	20	Nifedipine-d6	0.03 nM to 100 nM
Dehydro-nifedipine	positive	345.2	267.1	196	27	34	Nifedipine-d6	0.01 nM to 100 nM
Nifedipine-d6	positive	353.2	318.0	71	9	20	—	—
Diclofenac	positive	296.1	215.1	1	25	24	Diclofenac-d4	0.1 nM to 100 nM
4-hydroxy diclofenac	positive	313.8	230.0	76	47	32	Diclofenac-d4	0.1 nM to 100 nM
Diclofenac-d4	positive	296.1	215.1	1	25	24	—	—
Irinotecan	positive	587.2	123.9	231	41	16	Camptothecin	0.03 nM to 100 nM
SN-38	positive	393.2	349.2	81	33	38	Camptothecin	0.03 nM to 300 nM
Camptothecin	positive	349.2	305.1	161	31	38	—	—
Raloxifene	positive	474.2	112.1	246	39	10	Raloxifene-d4	0.03 nM to 30 nM
Raloxifene-4'-glucuronide	positive	650.2	474.2	206	19	16	Raloxifene-d4	0.03 nM to 100 nM
Raloxifene-6-glucuronide	positive	650.2	474.2	206	19	16	Raloxifene-d4	0.03 nM to 30 nM
Raloxifene-d4	positive	478.2	116.1	246	39	10	—	—

Supplementary Table 5. Summary of the estimated intestinal availability (Fg) for CYP3A substrates based on Eq. (7).

Data are presented as the mean ± S.D. (n = 3).

C_0 represents the initial concentration of test compound in the apical compartment.

ND; not detected

a; Varma et al. (2010)

Compounds	$Parent_{(Basolateral)}/C_0$ (μL/120 min)	$Metabolite_{(Apical + Intracellular + Basolateral)}/C_0$ (μL/120 min)	Estimated Fg value	In vivo human Fg value[a]
Felodipine	5.18 ± 0.78	10.3 ± 1.2	0.33 ± 0.02	0.35
Midazolam	73.1 ± 4.7	51.9 ± 6.3	0.59 ± 0.02	0.55
Nifedipine	87.6 ± 5.5	23.6 ± 2.7	0.79 ± 0.01	0.73
Triazolam	91.3 ± 5.2	1.49 ± 0.14	0.98 ± 0.00	0.74
Alprazolam	85.6 ± 4.1	N.D.	1	0.98